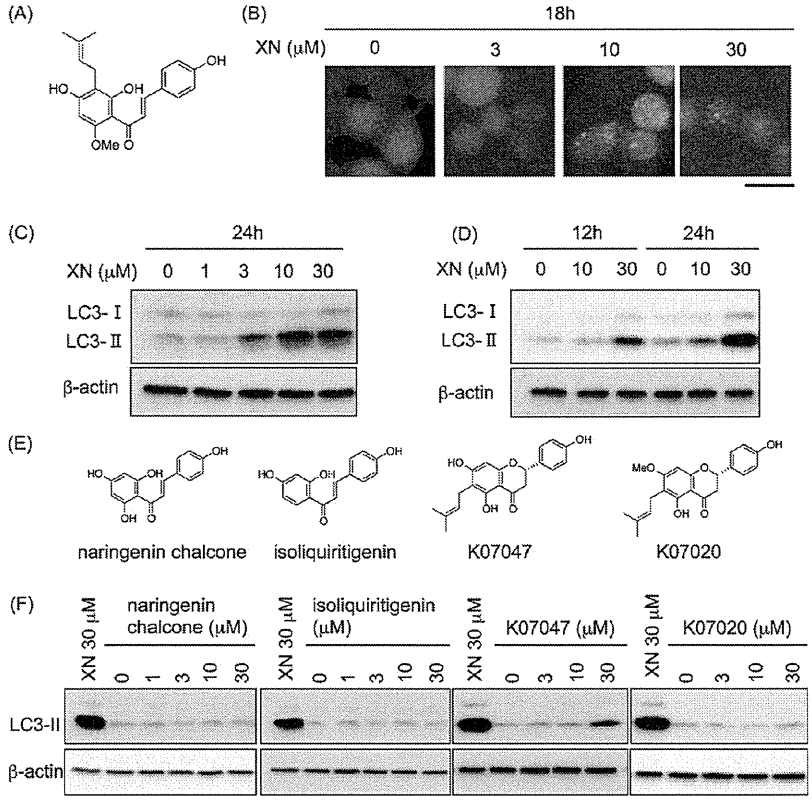

Figure 1. XN modulated autophagy. (A) Structure of xanthohumol (XN). (B) GFP-microtubule-associated protein 1 light chain 3 (LC3) stably expressing HeLa cells were treated with various concentrations of XN for 18 h. Cells were fixed with 3% (w/v) paraformaldehyde and observed under a fluorescence microscope (scale bar, 20 μm). (C) HeLa cells were treated with various concentrations of XN for 24 h. Cell lysates were immunoblotted with anti-LC3B antibody. β-Actin was immunoblotted as a loading control. (D) A431 cells were treated with various concentrations of XN for the indicated time. Cell lysates were immunoblotted with anti-LC3B antibody. β-Actin was immunoblotted as a loading control. (E) Structures of naringenin chalcone, isoliquiritigenin, K07047, and K07020. (F) A431 cells were treated with various concentrations of naringenin chalcone, isoliquiritigenin, K07047, or K07020 for 24 h. Cell lysates were immunoblotted with anti-LC3B antibody. β-Actin was immunoblotted as a loading control.

RESULTS AND DISCUSSION

Xanthohumol Inhibited Autophagosome Maturation.

In order to identify small compounds that could modulate autophagy and to explore the mechanism of autophagy through chemical genetics, we screened for a small compound from an in-house natural product library. As LC3-II is incorporated into the inner and outer surfaces of autophagosomes, the expression of a green fluorescence protein (GFP)-LC3 fusion protein can be used to identify GFP puncta representing autophagosomes.[17] Using this system to identify compounds that modulate autophagy, we searched for compounds that could increase the number of GFP-LC3 puncta in GFP-LC3 stably expressing human cervical carcinoma HeLa cells and found that xanthohumol (XN) showed this activity (Figure 1A). In untreated cells, GFP-LC3 was observed predominantly as diffuse green fluorescence in the cytoplasm. However, in XN-treated cells, characteristic punctate fluorescent patterns were observed, indicating that XN modulates autophagy in a dose-dependent manner, as shown in Figure 1B. Modulation of autophagy by XN was further confirmed by the detection of LC3-II, which is a phosphatidylethanolamine (PE) conjugated form of LC3, as a faster-migrating band when separated by SDS-PAGE and immunoblotted. As shown in Figure 1C, treatment of HeLa cells with XN for 24 h induced an increase in LC3-II levels in a dose-dependent manner. Similarly, XN increased LC3-II expression levels at 30 μM over 12–24 h in human epidermoid carcinoma A431 cells (Figure 1D). Next, we examined the effect of two other chalcones (naringenin chalcone and isoliquiritigenin) and two natural flavanones (K07047 and K07020) on LC3-II expression level. As a result, K07047 increased LC3-II levels weakly compared to XN, whereas naringenin chalcone, isoliquiritigenin, and K07020 did not increase LC3-II levels (Figure 1E,F)

The increase in LC3-II expression can be associated with either PE conjugation due to enhanced formation of autophagosomes or a block of LC3-II degradation due to impaired maturation of autophagosomes. To distinguish between these two possibilities, we detected expression levels of p62, a protein that is degraded by autophagy and accumulated when autophagy is impaired. Bafilomycin A1 (BMA) is known to prevent autophagosome maturation by inhibiting autophagosome-lysosome fusion[18] and caused an increase in the expression levels of p62 by inhibiting proteolytic degradation in autolysosomes, as shown in Figure 2A. Treatment with 30 μM XN for 24 h increased the expression levels of p62 as well. These data suggested that the increased LC3-II expression mediated by XN was a consequence of a block of autophagosome maturation. To further confirm that XN inhibited autophagosome maturation, we detected the localization of LC3 and lysosome in the presence of pepstatin A plus E64D, which are the lysosomal protease inhibitors, to inhibit the degradation of LC3 after fusion of autophagosome

dx.doi.org/10.1021/cb200492h | ACS Chem. Biol. XXXX, XXX, XXX–XXX

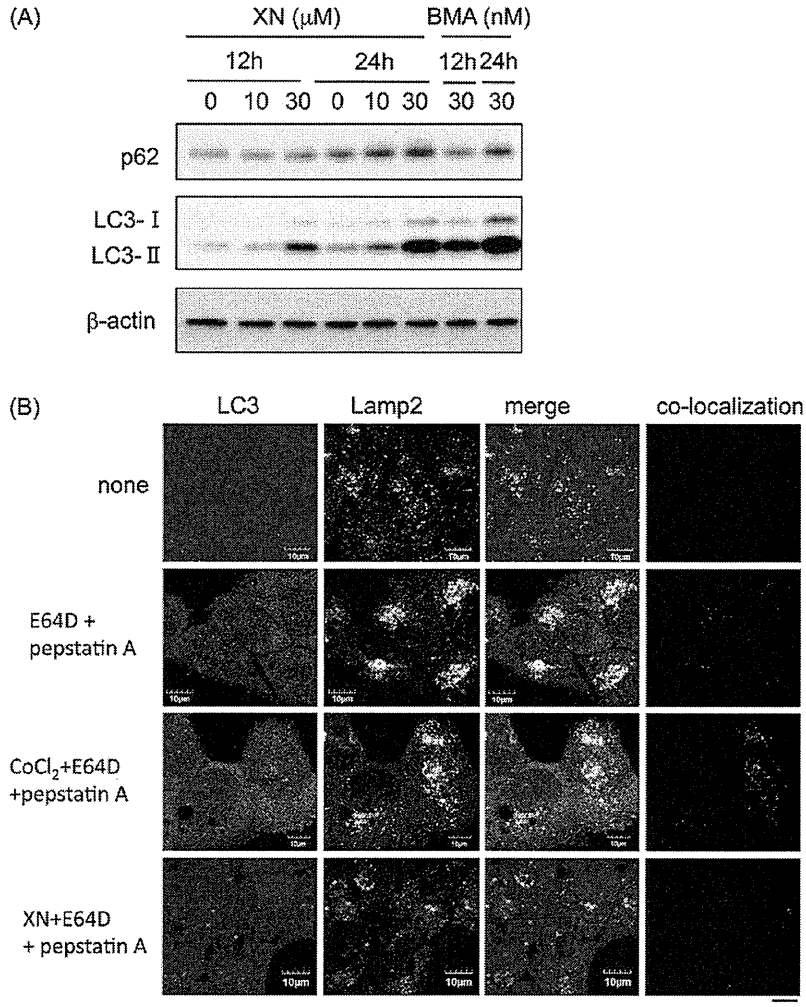

Figure 2. XN inhibited autophagosome maturation. (A) A431 cells were treated with various concentrations of XN or 30 nM bafilomycin A1 (BMA) for the indicated time. Cell lysates were immunoblotted with anti-p62 antibody. β-Actin was immunoblotted as a loading control. (B) A431 cells were treated with 30 μM XN or 0.3 mM $CoCl_2$ in the presence of 30 μM E64D and 30 μM pepstatin A for 24 h. Cells were then fixed with 3% (w/v) paraformaldehyde and immunostained with anti-LC3B and anti-lamp2 antibodies. The cells were observed under confocal microscopy (scale bar, 10 μm).

with lysosome. Because $CoCl_2$ are known to induce an increase in LC3-II expression levels by accelerating autophagosome formation,[19] we examined the effect of XN on the localization of LC3 and lysosome compared with the effect of $CoCl_2$. As shown in Figure 2B, $CoCl_2$ increased the number of LC3-positive puncta co-localizing with lysosome, whereas LC3-positive puncta increased by XN failed to co-localize with lysosome even in the presence of pepstatin A plus E64D. These data strongly indicated that XN impaired autophagosome maturation, resulting in increase in the level of LC3-II.

Identification of XN-Binding Proteins. To elucidate the underlying mechanism behind the suppression of autophagosome maturation induced by XN, we attempted to identify the cellular target protein of XN responsible for autophagy modulation. To this end, we used XN-immobilized agarose beads, which were prepared by a photocross-linking method.[20] A431 cell lysates were incubated for 3 h with XN-immobilized beads (XN beads) or control beads as a negative control. The reacted beads were washed, and the co-precipitated proteins were eluted, separated by SDS-PAGE, and stained with Coomassie brilliant blue (CBB). As shown in Figure 3A, four protein bands that specifically co-precipitated with XN beads were observed. Each protein band was identified by using MALDI-TOF-MS and LC–MS/MS as (i) valosin-containing protein (VCP), (ii) voltage-dependent anion channel (VDAC), (iii) prohibitin-2, and (iv) prohibitin.

Among these proteins, competition was observed only for VCP with 0.1–1 μmol XN as shown in Figure 3B. VCP has been reported to play a role in the maturation of autophagosomes.[21,22] VCP, also known as p97, is one of the best-characterized type II AAA (ATPases associated with diverse cellular activities) ATPases. VCP plays critical roles in a broad range of diverse cellular processes, including ER associated degradation *via* the ubiquitin-proteasome system,[23,24] cell cycle regulation,[25] and DNA repair.[26] Recently, it was reported that VCP is essential for autophagosome–lysosome fusion and formation of autolysosomes in human cell lines.[21,22] Therefore, we speculated that VCP might be the target of XN, and the binding of XN to VCP was confirmed by immunoblotting of co-precipitated protein from XN-beads using anti-VCP antibody (Figure 3C).

XN Bound Directly to the N Domain of VCP. Next, to determine whether XN could bind directly to VCP, we performed an *in vitro* binding assay using purified recombinant

dx.doi.org/10.1021/cb200492h | *ACS Chem. Biol.* XXXX, XXX, XXX–XXX

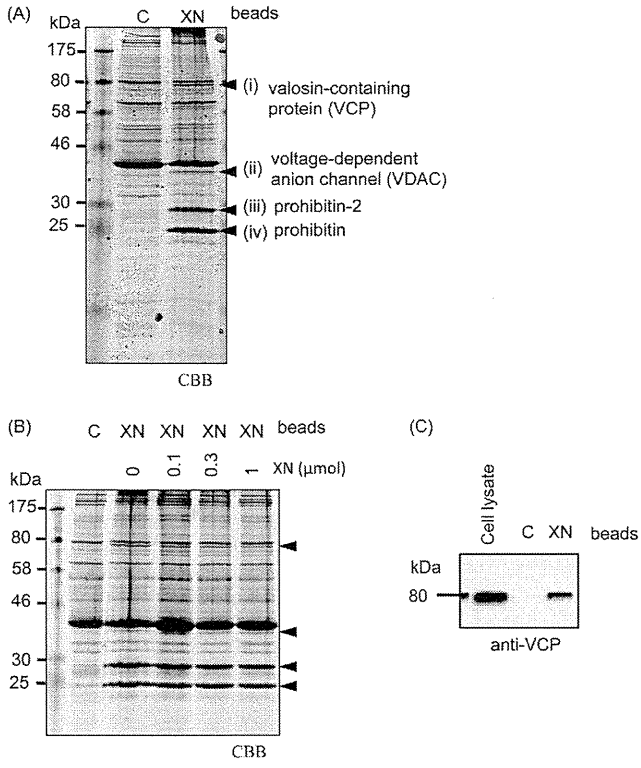

Figure 3. Identification of XN-binding proteins. (A) A431 cell lysates were incubated with control beads or XN beads for 3 h. The reacted beads were washed, and the eluted proteins were subjected to SDS-PAGE and stained by Coomassie brilliant blue (CBB). The co-precipitated proteins for XN beads were identified by using MALDI-TOF-MS and LC–MS/MS. (B) A431 cell lysates were preincubated with 0.1–1 μmol of XN as a competitor for 1 h and then incubated with control beads or XN beads for 3 h. The reacted beads were washed, and the eluted proteins were subjected to SDS-PAGE and stained by CBB. (C) A431 cell lysates were incubated with control beads or XN beads for 3 h. The reacted beads were washed, and the eluted proteins were immunoblotted with anti-valosin-containing protein (VCP) antibody.

GST-tagged VCP protein. Unlike GST, GST-VCP was co-precipitated only with XN-beads, as shown in Figure 4A. Moreover, competition was observed for VCP in the presence of 0.5 μmol of XN (Figure 4B), indicating that XN binds directly to VCP. On the other hand, competition was not observed for binding of XN-beads and VCP in the presence of XN analogues such as naringenin chalcone, isoliquiritigenin, K07047, and K07020 up to 0.5 μmol (Figure 4C), indicating that these analogues bind to VCP very weakly or fail to bind to VCP at least through the XN binding site. Because these analogues fail to induce LC3-II expression level or induce it very weakly, these observations further confirm the importance of the XN binding to VCP for impairment of autophagosome maturation. In addition, because naringenin chalcone and isoliquiritigenin did not bind to VCP, the prenyl and/or *O*-methyl group of XN is thought to be important for binding to VCP.

VCP is composed of a substrate and cofactor binding N domain followed by two AAA ATPase domains, termed D1 and D2, and forms a hexameric double-ring structure.[27,28] It has been demonstrated that both D1 and D2 domain contain Walker A and Walker B motifs that mediate ATP binding and hydrolysis, respectively. However, these two ATPase domains are not catalytically equivalent: D2 domain has the major ATPase activity at physiological temperatures, whereas D1 is involved in the regulation of heat-induced ATPase activity.[29] D1 also plays a major role in hexamerization.[30,31] To determine which domain in VCP is essential for interaction with XN, we prepared three GST-tagged VCP mutants that lacked the N-terminal domain (1–185) (GST-VCPΔN), D1 domain containing Walker A and Walker B motifs (186–348) (GST-VCPΔD1), and D2 domain containing Walker A and Walker B motifs (349–806) (GST-VCPΔD2) (Figure 4D). GST-VCPΔD1 and GST-VCPΔD2 were co-precipitated with XN beads, whereas GST-VCPΔ*N* was not, as shown in Figure 4E. These results indicated that XN bound to the N domain of VCP.

XN Inhibited VCP Function. Next, we examined whether this binding of XN to the N domain of VCP could inhibit VCP function. The structural alteration of the N domain of VCP has been reported to induce impaired maturation of autophagosome as well as impaired ER associated degradation (ERAD),[32] and loss of VCP-mediated ERAD activity leads to accumulation of unfolded protein in the ER, resulting in induction of ER stress.[33] Therefore, we examined the effect of XN on the expression of the ER stress markers CHOP and GRP78. As shown in Figure 5A, treatment with 30 μM XN for 12–24 h increased the protein levels of CHOP and GRP78 significantly in A431 cells, suggesting that XN inhibited VCP-mediated ERAD. On the other hand, Hirabayashi *et al.* reported that inhibition of VCP function by using dominant negative VCP induced cytoplasmic vacuolation.[34] These vacuoles are reported to be a result of abnormal budding and enlargement of the ER.[35] We also observed the presence of microscopic vacuoles not only in VCP knockdown A431 cells by using siRNA (Figure 5B) but also in XN-treated A431 cells (Figure 5C). The successful knockdown of VCP using siRNA and resultant up-regulation of LC3-II was confirmed by immunoblotting, as shown in Figure 5B right. Moreover, the XN analogue K07047, which modulated autophagy weakly, also induced vacuolization weakly compared with XN. On the other hand, other analogues including naringenin chalcone, isoliquiritigenin, and K07020, which had no effect on modulation of autophagy, did not induce vacuolization (Figures 1F and 5C). Taken together, these data indicated that XN bound to the N domain of VCP directly, thereby suppressing VCP function.

Apart from autophagy, XN has been reported to inhibit mitogen/antigen-induced T cell proliferation, development of cell-mediated cytotoxicity, and production of Th1 cytokines by inhibiting NF-κB.[36] Moreover, XN has been shown to inhibit the growth of a wide variety of human cancer cell lines by inhibiting proliferation and inducing apoptosis.[37,38] These previous observations regarding XN suggested the following two possibilities: one possible explanation is that various proteins were interfered with by XN and various biological phenomena were affected, and the other is that XN modulated a specific protein, which was involved in the various biological processes. Our finding that XN modulated the function of VCP may explain how XN exhibited the above-mentioned effects, because VCP is reported to play important roles in the degradation of IκB, resulting in enhancement of NF-κB signaling,[39,40] or because the expression level of VCP is correlated with progression, prognosis, and recurrence of certain types of cancer.[41,42]

Two types of VCP inhibitors have been reported in the literature. The first type of inhibitor is classified as a VCP

dx.doi.org/10.1021/cb200492h | *ACS Chem. Biol.* XXXX, XXX, XXX–XXX

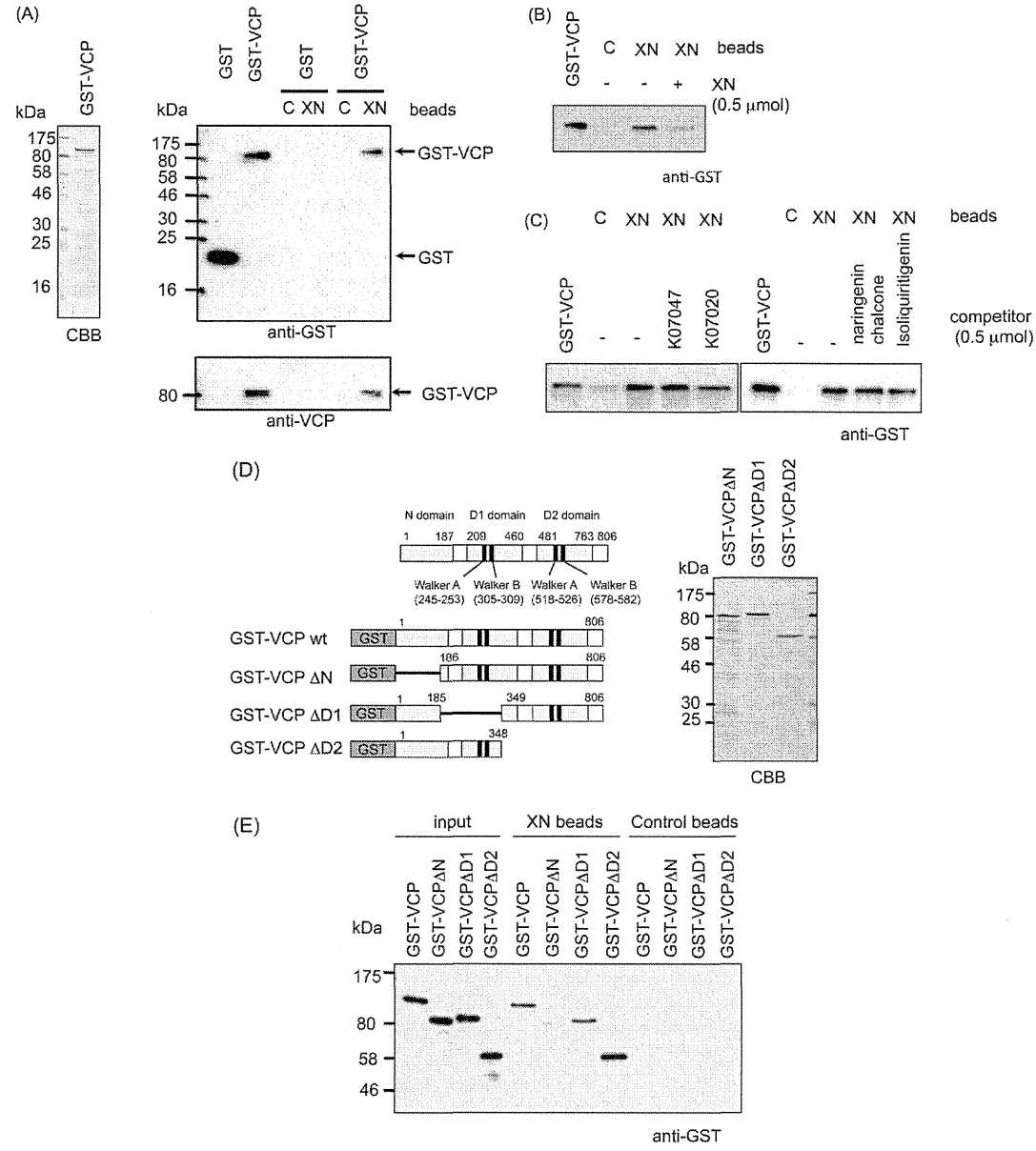

Figure 4. XN bound directly to the N domain of VCP. (A) (left) CBB staining of purified GST-VCP protein. (right) Purified GST and GST-tagged VCP were incubated with control beads or XN beads for 3 h. The reacted beads were washed, and the eluted proteins were immunoblotted with anti-GST and anti-VCP antibodies. (B) Purified GST-tagged VCP was preincubated with 0.5 μmol of XN as a competitor for 1 h and then incubated with control beads or XN beads for 3 h. The reacted beads were washed, and the eluted proteins were immunoblotted with anti-GST antibody. (C) Purified GST-tagged VCP was preincubated with 0.5 μmol of naringenin chalcone, isoliquiritigenin, K07047, or K07020 as a competitor for 1 h and then incubated with control beads or XN beads for 3 h. The reacted beads were washed, and the eluted proteins were immunoblotted with anti-GST antibody. (D) (left) Schematic illustration of GST-VCP, GST-VCPΔN, GST-VCPΔD1, and GST-VCPΔD2. (right) CBB staining of purified GST-VCPΔN, GST-VCPΔD1, and GST-VCPΔD2. (E) Purified GST-VCPΔN, GST-VCPΔD1, and GST-VCPΔD2 were incubated with control beads or XN beads for 3 h. The reacted beads were washed, and the eluted proteins were immunoblotted with anti-GST antibody.

ATPase inhibitor, which most likely binds to a site in the D2 ATPase domain. 2-Anilino-4-aryl-1,3-thiazoles were discovered by high-throughput screening (HTS) as inhibitors of VCP ATPase activity, and these were reported to inhibit VCP-associated protein degradation.[43] Syk inhibitor III was reported to be an irreversible inhibitor of VCP ATPase activity by interacting with Cys522 within the D2 ATPase domain of VCP and the ubiquitin-fused reporter protein.[44] N^2,N^4-Dibenzylquinazoline-2,4-diamine (DBeQ) was identified as a selective, potent, reversible, and ATP-competitive VCP inhibitor by screening a library of chemical compounds.[45] DBeQ blocks multiple processes that have been shown by siRNA to depend on VCP, including degradation of ubiquitin fusion degradation and ERAD as well as autophagosomal maturation. The second type of VCP inhibitor is Eeyarestatin I (Eer I), which binds to the D1 domain of VCP without affecting ATPase activity.[46] Eer I was found to directly associate with the ER membrane and VCP and inhibited VCP-associated deubiquitinating enzymes, thereby inhibiting VCP-dependent protein degradation. However, so far, VCP inhibitors that bind to the N domain of VCP have not yet been reported. Therefore, XN is the first example of such an inhibitor that binds to the N domain of VCP and

dx.doi.org/10.1021/cb200492h | ACS Chem. Biol. XXXX, XXX, XXX–XXX

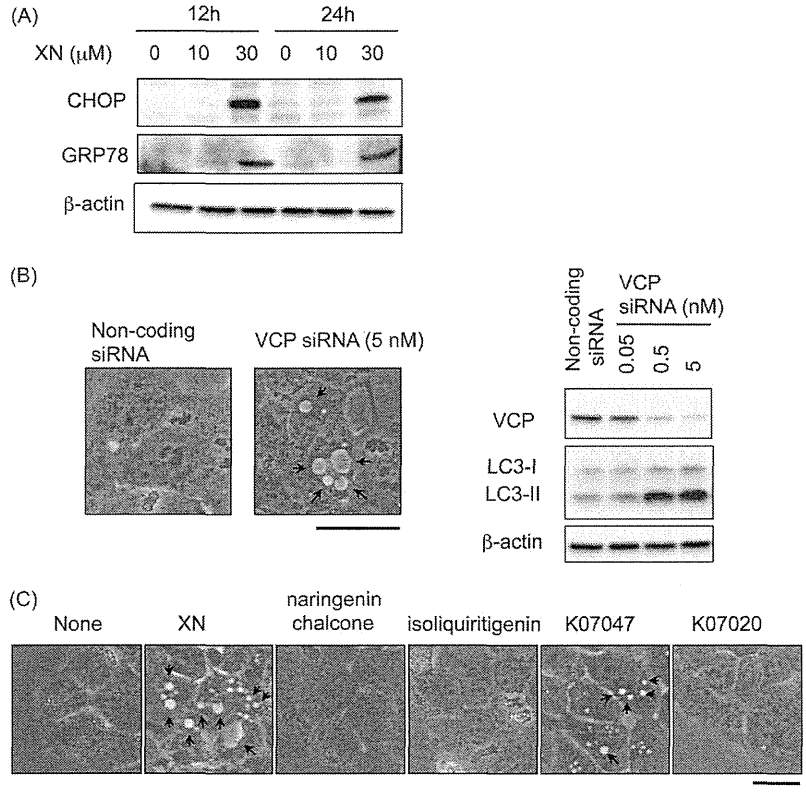

Figure 5. XN inhibited VCP function. (A) A431 cells were treated with various concentrations of XN for the indicated time. Cell lysates were immunoblotted with anti-CHOP and anti-GRP78 antibodies. β-Actin was immunoblotted as a loading control. (B) (left) A431 cells were observed under a microscope 72 h after transfection with non-coding siRNA or VCP siRNA (arrows, vacuoles; scale bar, 25 μm). (right) A431 cells were transfected with VCP siRNA or noncoding siRNA for 72 h. Cell lysates were immunoblotted with anti-VCP and anti-LC3B antibodies. β-Actin was immunoblotted as a loading control. (C) A431 cells were treated with 30 μM XN, naringenin chalcone, isoliquiritigenin, K07047, or K07020 for 24 h and then observed under microscope (arrows, vacuoles; scale bar, 25 μm).

inactivates VCP. Thus, XN is proposed to be a new class of VCP inhibitors, which may be used as a powerful tool for identifying the cofactor or substrate protein of VCP responsible for autophagy regulation.

METHODS

Reagents. Naringenin chalcone was obtained as a generous gift from Kikkoman Corporation. Isoliquiritigenin, E64D, and peptatin A were purchased from Sigma-Aldrich Co.

Cell Line. Human epidermoid carcinoma A431 cells were grown in Dulbecco's modified Eagle medium supplemented with 5% (v/v) calf serum, 100 U mL^{-1} of penicillin G (Sigma-Aldrich Co.), and 0.1 mg mL^{-1} of kanamycin (Sigma-Aldrich Co.) at 37 °C in a 5% CO_2–95% air atmosphere. Human cervical carcinoma HeLa cells were grown in Dulbecco's modified Eagle's medium supplemented with 8% fetal bovine serum, 100 U mL^{-1} of penicillin G, and 0.1 mg mL^{-1} of kanamycin at 37 °C in a 5% CO_2–95% air atmosphere. HeLa/GFP-LC3 stable cell lines were established as previously described.[47]

Isolation of XN from Hop and XN Analogues from Microbial Origin. XN was isolated from commercially available hop extract obtained from Hopsteiner. The extract (200 mg) was purified by using preparative octadecylsilyl (ODS) HPLC (UG 80, 20 mm, 250 mm; SHISEIDO) with 70% (v/v) aqueous MeOH to obtain pure XN (147 mg). The structures were identified by spectroscopic data (NMR and MS). UV (MeOH) λ_{max} (log ε) 369 (4.56); ESIMS m/z 355 $[M + H]^+$; ^{13}C NMR δ192.8, 165.5, 161.8, 161.2, 157.4, 142.0, 136.0, 130.3 (2C), 128.6, 125.5, 121.7, 116.2 (2C), 106.3, 106.2, 105.0, 56.1, 25.8, 21.6, and 17.9. K07020 and K07047 were isolated from 14 L of culture broths of *Streptomyces* sp. HK-803 and *Streptomyces spiroverticillatus* JC-8444 by UV absorption and mass spectra guided separation to afford 10.6 and 9.3 mg as a pale-yellow powder, respectively. The structures were identified by spectroscopic data (NMR and MS). K07020: UV (MeOH) λ_{max} (log ε) 226 (4.45), 288 nm (4.33); ESIMS m/z 353 $[M - H]^-$; ^{13}C NMR δ192.9, 164.6, 163.8, 161.8, 158.8, 131.6, 131.5, 128.9 (2C), 123.9, 116.2 (2C), 110.0, 105.7, 93.5, 80.0, 55.9, 46.2, 26.0, 22.7, and 17.9. K07047: UV (MeOH) λ_{max} (log ε) 226 (4.36), 293 nm (4.24); ESIMS m/z 339 $[M - H]^-$; ^{13}C NMR δ197.8, 165.9, 162.6, 162.5, 159.0, 131.5, 131.2, 129.0 (2C), 123.9, 116.3 (2C), 109.6, 103.2, 95.4, 80.4, 44.2, 25.9, 21.8, and 17.8.

DNA Constructs. Human cDNA for VCP were amplified from A431 cell cDNA and subcloned into pGEX-2T (GE Healthcare UK Ltd.) to prepare GST fusion proteins in bacteria. Expression vectors encoding GST-fused VCP mutants (ΔN, 1–185 aa deletion; ΔD_1, 186–348 aa deletion; and ΔD_2, 349–806 aa deletion) were generated by PCR using pGEX-2T/VCP as a template.

Fluorescence Microscopy. For fluorescence microscopy, HeLa cells stably expressing GFP-LC3, which were grown on coverslips, were treated with chemicals for the indicated time at 37 °C. Cells were fixed with 3% (w/v) paraformaldehyde in PBS at RT. The cells were then washed with PBS and observed under a fluorescence microscope (Olympus).

Western blotting. Cells were lysed with RIPA buffer [25 mM HEPES, 1.5% (v/v) TX-100, 1% (w/v) sodium deoxycholate, 0.1% (w/v) SDS, 0.5 M NaCl, 5 mM EDTA, 50 mM NaF, 100 mM Na_3VO_4, 0.1 mg mL^{-1} leupeptin, 1 mM PMSF; pH 7.8]. Proteins were separated by SDS-PAGE, transferred to a PVDF membrane (Millipore), and probed with specific antibodies. This was followed by detection using the ECL Western blotting detection system (Millipore) and LAS-1000 (Fuji Film). The primary antibodies used were as follows: anti-LC3B (L7543, Sigma-Aldrich Co.), anti-β-actin (AC-74, Sigma-Aldrich Co.), anti-p62 (5114, Cell Signaling Technology), anti-VCP (ab 11433, Abcam), anti-GST (B-14, Santa

dx.doi.org/10.1021/cb200492h | ACS Chem. Biol. XXXX, XXX, XXX–XXX

Cruz Biotechnology), anti-GRP78 (H-129, Santa Cruz Biotechnology), and anti-CHOP (MA1-250, Thermo Fisher Scientific Inc.) antibodies. The secondary antibodies were horseradish peroxidase-conjugated anti-mouse IgG and anti-rabbit IgG (GE Healthcare UK Ltd.).

Immunofluorescent Microscopy. Immunofluorescent microscopy was carried out as previously described.[48] Fluorescence images were obtained using a confocal laser scanning microscope system FV1000 (Olympus).

Detection of Binding Proteins for XN Beads. XN beads were prepared as previously described.[20] A431 cells were harvested, washed with PBS, and then resuspended in binding buffer [50 mM HEPES, 150 mM NaCl, 2.5 mM EGTA, 1 mM EDTA, 1 mM DTT, 0.1 mM PMSF, NP40 1% (v/v) and protease inhibitor cocktail tablets (Roche); pH 7.5]. After cells were lysed by homogenization with sonication, the insoluble material was removed by centrifugation, and the supernatant was collected as cell lysate. The cell lysate (3 mg of protein) was then incubated with XN beads (20 μL) for 3 h at 4 °C. The reacted beads were washed with binding buffer, and the binding proteins were eluted with SDS-PAGE sample buffer, separated by SDS-PAGE, and visualized by CBB staining. Identification of the proteins was performed using MALDI-TOF-MS and LC−MS/MS as previously described.[49]

***In Vitro* XN Beads Pull-Down Assay.** GST fusion proteins, which were expressed in the *Escherichia coli* BL21 strain and purified using Glutathione Sepharose 4B (GE Healthcare UK Ltd.), were incubated with XN beads in 1 mL of binding buffer for 3 h. The beads were washed with binding buffer and eluted with SDS-PAGE sample buffer. The eluted proteins were then subjected to SDS-PAGE. For the competition assay, each compound was added 1 h before incubation with XN beads.

RNA Interference. siRNA double-stranded oligonucleotides designed to interfere with the expression of VCP (sense 5′-UAGAACAGAACUCCCUUGGAAGGUG-3′; Invitrogen) and non-coding siRNA (Invitrogen) as a negative control were used. Reverse transfection was demonstrated by using HiPerFect (QIAGEN) according to the manufacturer's instructions. Briefly, A431 cells were trypsinized, resuspended in antibiotic-free medium, mixed with OPTI-MEM (Gibco) including siRNA and HiPerFect, and then seeded onto a 12-well plate. 72 h after transfection, cells were observed under microscope and lysed for Western blotting.

■ ASSOCIATED CONTENT

Accession Codes

Uni-Prot accession codes are described as following; valosion-containg protein (TERA_HUMAN), P55072; voltage-dependent anion channel (VDAC1_HUMAN), P21796; Prohibitin 2 (PHB2_HUMAN), Q99623; Prohibitin (PHB_HUMAN), P35232

■ AUTHOR INFORMATION

Corresponding Author

*E-mail: imoto@bio.keio.ac.jp.

Author Contributions

#These authors contributed equally to this work.

Notes

The authors declare no competing financial interest.

■ ACKNOWLEDGMENTS

We thank K. Honda (RIKEN, Japan) for preparing XN-beads; H. Kondo (RIKEN, Japan) for identification of XN-binding protein; S. Saiki (Juntendo University, Japan), M. Ueki, Y. Futamura, T. Saito (RIKEN, Japan) and S. Shinjo (Keio University, Japan) for technical advice; Kikkoman Corporation for kindly providing us with naringenin chalcone. We are very grateful for a grant from Hayashi Memorial Foundation for Female Natural Scientists and a scholarship from Suntory Institute for Bioorganic Research. This work was supported by a Grant-in-Aid for Scientific Research (B) and JSPS Fellows, the Ministry of Education, Culture, Sports, Science, and Technology,

■ REFERENCES

(1) Ohsumi, Y. (2001) Molecular dissection of autophagy: two ubiquitin-like systems. *Nat. Rev. Mol. Cell Biol. 2*, 211−216.

(2) Yoshimori, T. (2004) Autophagy: a regulated bulk degradation process inside cells. *Biochem. Biophys. Res. Commun. 313*, 453−458.

(3) Martinez-Vicente, M., Talloczy, Z., Wong, E., Tang, G., Koga, H., Kaushik, S., de Vries, R., Arias, E., Harris, S., Sulzer, D., and Cuervo, A. M. (2010) Cargo recognition failure is responsible for inefficient autophagy in Huntington's disease. *Nat. Neurosci. 13*, 567−576.

(4) Matsuda, N., and Tanaka, K. (2009) Does impairment of the ubiquitin-proteasome system or the autophagy-lysosome pathway predispose individuals to neurodegenerative disorders such as Parkinson's disease? *J. Alzheimer's Dis. 19*, 1−9.

(5) Mathew, R., Karantza-Wadsworth, V., and White, E. (2007) Role of autophagy in cancer. *Nat. Rev. Cancer 7*, 961−967.

(6) Ebato, C., Uchida, T., Arakawa, M., Komatsu, M., Ueno, T., Komiya, K., Azuma, K., Hirose, T., Tanaka, K., Kominami, E., Kawamori, R., Fujitani, Y., and Watada, H. (2008) Autophagy is important in islet homeostasis and compensatory increase of beta cell mass in response to high-fat diet. *Cell Metab. 8*, 325−332.

(7) Tsukada, M., and Ohsumi, Y. (1993) Isolation and characterization of autophagy-defective mutants of *Saccharomyces cerevisiae*. *FEBS Lett. 333*, 169−174.

(8) Klionsky, D. J., Cregg, J. M., Dunn, W. A. Jr., Emr, S. D., Sakai, Y., Sandoval, I. V., Sibirny, A., Subramani, S., Thumm, M., Veenhuis, M., and Ohsumi, Y. (2003) A unified nomenclature for yeast autophagy-related genes. *Dev. Cell 5*, 539−545.

(9) Lum, J. J., DeBerardinis, R. J., and Thompson, C. B. (2005) Autophagy in metazoans: cell survival in the land of plenty. *Nat. Rev. Mol. Cell Biol. 6*, 439−448.

(10) Blommaart, E. F., Krause, U., Schellens, J. P., Vreeling-Sindelarova, H., and Meijer, A. J. (1997) The phosphatidylinositol 3-kinase inhibitors wortmannin and LY294002 inhibit autophagy in isolated rat hepatocytes. *Eur. J. Biochem. 243*, 240−246.

(11) Power, B. F. B., Tutin, F., and Rogerson, H. (1913) CXXXV. The constituents of Hops. *J. Chem. Soc., Trans. 103*, 1267−1292.

(12) Tabata, N., Ito, M., Tomoda, H., and Omura, S. (1997) Xanthohumols, diacylglycerol acyltransferase inhibitors, from *Humulus lupulus*. *Phytochemistry 46*, 683−687.

(13) Inokoshi, J., Kawamoto, K., Takagi, Y., Matsuhama, M., Omura, S., and Tomoda, H. (2009) Expression of two human acyl-CoA:diacylglycerol acyltransferase isozymes in yeast and selectivity of microbial inhibitors toward the isozymes. *J Antibiot. (Tokyo) 62*, 51−54.

(14) Gerhauser, C., Alt, A., Heiss, E., Gamal-Eldeen, A., Klimo, K., Knauft, J., Neumann, I., Scherf, H. R., Frank, N., Bartsch, H., and Becker, H. (2002) Cancer chemopreventive activity of xanthohumol, a natural product derived from hop. *Mol. Cancer Ther. 1*, 959−969.

(15) Albini, A., Dell'Eva, R., Vene, R., Ferrari, N., Buhler, D. R., Noonan, D. M., and Fassina, G. (2006) Mechanisms of the antiangiogenic activity by the hop flavonoid xanthohumol: NF-kappaB and Akt as targets. *FASEB J. 20*, 527−529.

(16) Lust, S., Vanhoecke, B., Van Gele, M., Boelens, J., Van Melckebeke, H., Kaileh, M., Vanden Berghe, W., Haegeman, G., Philippe, J., Bracke, M., and Offner, F. (2009) Xanthohumol activates the proapoptotic arm of the unfolded protein response in chronic lymphocytic leukemia. *Anticancer Res. 29*, 3797−3805.

(17) Kabeya, Y., Mizushima, N., Ueno, T., Yamamoto, A., Kirisako, T., Noda, T., Kominami, E., Ohsumi, Y., and Yoshimori, T. (2000) LC3, a mammalian homologue of yeast Apg8p, is localized in autophagosome membranes after processing. *EMBO J. 19*, 5720−5728.

(18) Yamamoto, A., Tagawa, Y., Yoshimori, T., Moriyama, Y., Masaki, R., and Tashiro, Y. (1998) Bafilomycin A1 prevents maturation of autophagic vacuoles by inhibiting fusion between autophagosomes and lysosomes in rat hepatoma cell line, H-4-II-E cells. *Cell Struct. Funct. 23*, 33–42.

(19) Vigneswaran, N., Wu, J., Song, A., Annapragada, A., and Zacharias, W. (2011) Hypoxia-induced autophagic response is associated with aggressive phenotype and elevated incidence of metastasis in orthotopic immunocompetent murine models of head and neck squamous cell carcinomas (HNSCC). *Exp. Mol. Pathol. 90*, 215–225.

(20) Kanoh, N., Honda, K., Simizu, S., Muroi, M., and Osada, H. (2005) Photo-cross-linked small-molecule affinity matrix for facilitating forward and reverse chemical genetics. *Angew. Chem., Int. Ed.. 44*, 3559–3562.

(21) Ju, J. S., Fuentealba, R. A., Miller, S. E., Jackson, E., Piwnica-Worms, D., Baloh, R. H., and Weihl, C. C. (2009) Valosin-containing protein (VCP) is required for autophagy and is disrupted in VCP disease. *J. Cell Biol. 187*, 875–888.

(22) Tresse, E., Salomons, F. A., Vesa, J., Bott, L. C., Kimonis, V., Yao, T. P., Dantuma, N. P., and Taylor, J. P. (2010) VCP/p97 is essential for maturation of ubiquitin-containing autophagosomes and this function is impaired by mutations that cause IBMPFD. *Autophagy 6*, 217–227.

(23) Ye, Y., Meyer, H. H., and Rapoport, T. A. (2001) The AAA ATPase Cdc48/p97 and its partners transport proteins from the ER into the cytosol. *Nature 414*, 652–656.

(24) Jarosch, E., Taxis, C., Volkwein, C., Bordallo, J., Finley, D., Wolf, D. H., and Sommer, T. (2002) Protein dislocation from the ER requires polyubiquitination and the AAA-ATPase Cdc48. *Nat. Cell Biol. 4*, 134–139.

(25) Mouysset, J., Deichsel, A., Moser, S., Hoege, C., Hyman, A. A., Gartner, A., and Hoppe, T. (2008) Cell cycle progression requires the CDC-48UFD-1/NPL-4 complex for efficient DNA replication. *Proc. Natl. Acad. Sci. U.S.A. 105*, 12879–12884.

(26) Partridge, J. J., Lopreiato, J. O. Jr., Latterich, M., and Indig, F. E. (2003) DNA damage modulates nucleolar interaction of the Werner protein with the AAA ATPase p97/VCP. *Mol. Biol. Cell 14*, 4221–4229.

(27) Rouiller, I., DeLaBarre, B., May, A. P., Weis, W. I., Brunger, A. T., Milligan, R. A., and Wilson-Kubalek, E. M. (2002) Conformational changes of the multifunction p97 AAA ATPase during its ATPase cycle. *Nat. Struct. Biol. 9*, 950–957.

(28) DeLaBarre, B., and Brunger, A. T. (2003) Complete structure of p97/valosin-containing protein reveals communication between nucleotide domains. *Nat. Struct. Biol. 10*, 856–863.

(29) Song, C., Wang, Q., and Li, C. C. (2003) ATPase activity of p97-valosin-containing protein (VCP). D2 mediates the major enzyme activity, and D1 contributes to the heat-induced activity. *J. Biol. Chem. 278*, 3648–3655.

(30) Wang, Q., Song, C., and Li, C. C. (2003) Hexamerization of p97-VCP is promoted by ATP binding to the D1 domain and required for ATPase and biological activities. *Biochem. Biophys. Res. Commun. 300*, 253–260.

(31) Wang, Q., Song, C., Yang, X., and Li, C. C. (2003) D1 ring is stable and nucleotide-independent, whereas D2 ring undergoes major conformational changes during the ATPase cycle of p97-VCP. *J. Biol. Chem. 278*, 32784–32793.

(32) Yamanaka, K., Sasagawa, Y., and Ogura, T. (2012) Recent advances in p97/VCP/Cdc48 cellular functions. *Biochim. Biophys. Acta 1823*, 130–137.

(33) Wojcik, C., Rowicka, M., Kudlicki, A., Nowis, D., McConnell, E., Kujawa, M., and DeMartino, G. N. (2006) Valosin-containing protein (p97) is a regulator of endoplasmic reticulum stress and of the degradation of N-end rule and ubiquitin-fusion degradation pathway substrates in mammalian cells. *Mol. Biol. Cell 17*, 4606–4618.

(34) Hirabayashi, M., Inoue, K., Tanaka, K., Nakadate, K., Ohsawa, Y., Kamei, Y., Popiel, A. H., Sinohara, A., Iwamatsu, A., Kimura, Y., Uchiyama, Y., Hori, S., and Kakizuka, A. (2001) VCP/p97 in abnormal protein aggregates, cytoplasmic vacuoles, and cell death, phenotypes relevant to neurodegeneration. *Cell Death Differ. 8*, 977–984.

(35) Kobayashi, T., Tanaka, K., Inoue, K., and Kakizuka, A. (2002) Functional ATPase activity of p97/valosin-containing protein (VCP) is required for the quality control of endoplasmic reticulum in neuronally differentiated mammalian PC12 cells. *J. Biol. Chem. 277*, 47358–47365.

(36) Gao, X., Deeb, D., Liu, Y., Gautam, S., Dulchavsky, S. A., and Gautam, S. C. (2009) Immunomodulatory activity of xanthohumol: inhibition of T cell proliferation, cell-mediated cytotoxicity and Th1 cytokine production through suppression of NF-kappaB. *Immunopharmacol. Immunotoxicol. 31*, 477–484.

(37) Pan, L., Becker, H., and Gerhauser, C. (2005) Xanthohumol induces apoptosis in cultured 40–16 human colon cancer cells by activation of the death receptor- and mitochondrial pathway. *Mol. Nutr. Food Res. 49*, 837–843.

(38) Deeb, D., Gao, X., Jiang, H., Arbab, A. S., Dulchavsky, S. A., and Gautam, S. C. (2010) Growth inhibitory and apoptosis-inducing effects of xanthohumol, a prenylated chalone present in hops, in human prostate cancer cells. *Anticancer Res. 30*, 3333–3339.

(39) Dai, R. M., Chen, E., Longo, D. L., Gorbea, C. M., and Li, C. C. (1998) Involvement of valosin-containing protein, an ATPase Co-purified with IkappaBalpha and 26 S proteasome, in ubiquitin-proteasome-mediated degradation of IkappaBalpha. *J. Biol. Chem. 273*, 3562–3573.

(40) Asai, T., Tomita, Y., Nakatsuka, S., Hoshida, Y., Myoui, A., Yoshikawa, H., and Aozasa, K. (2002) VCP (p97) regulates NFkappaB signaling pathway, which is important for metastasis of osteosarcoma cell line. *Jpn. J. Cancer Res. 93*, 296–304.

(41) Yamamoto, S., Tomita, Y., Hoshida, Y., Takiguchi, S., Fujiwara, Y., Yasuda, T., Yano, M., Nakamori, S., Sakon, M., Monden, M., and Aozasa, K. (2003) Expression level of valosin-containing protein is strongly associated with progression and prognosis of gastric carcinoma. *J. Clin. Oncol. 21*, 2537–2544.

(42) Yamamoto, S., Tomita, Y., Uruno, T., Hoshida, Y., Qiu, Y., Iizuka, N., Nakamichi, I., Miyauchi, A., and Aozasa, K. (2005) Increased expression of valosin-containing protein (p97) is correlated with disease recurrence in follicular thyroid cancer. *Ann. Surg. Oncol. 12*, 925–934.

(43) Bursavich, M. G., Parker, D. P., Willardsen, J. A., Gao, Z. H., Davis, T., Ostanin, K., Robinson, R., Peterson, A., Cimbora, D. M., Zhu, J. F., and Richards, B. (2010) 2-Anilino-4-aryl-1,3-thiazole inhibitors of valosin-containing protein (VCP or p97). *Bioorg. Med. Chem. Lett. 20*, 1677–1679.

(44) Chou, T. F., and Deshaies, R. J. (2011) Quantitative cell-based protein degradation assays to identify and classify drugs that target the ubiquitin-proteasome system. *J. Biol. Chem. 286*, 16546–16554.

(45) Chou, T. F., Brown, S. J., Minond, D., Nordin, B. E., Li, K., Jones, A. C., Chase, P., Porubsky, P. R., Stoltz, B. M., Schoenen, F. J., Patricelli, M. P., Hodder, P., Rosen, H., and Deshaies, R. J. (2011) Reversible inhibitor of p97, DBeQ, impairs both ubiquitin-dependent and autophagic protein clearance pathways. *Proc. Natl. Acad. Sci. U.S.A. 108*, 4834–4839.

(46) Wang, Q., Shinkre, B. A., Lee, J. G., Weniger, M. A., Liu, Y., Chen, W., Wiestner, A., Trenkle, W. C., and Ye, Y. (2010) The ERAD inhibitor Eeyarestatin I is a bifunctional compound with a membrane-binding domain and a p97/VCP inhibitory group. *PLoS One 5*, e15479.

(47) Balgi, A. D., Fonseca, B. D., Donohue, E., Tsang, T. C., Lajoie, P., Proud, C. G., Nabi, I. R., and Roberge, M. (2009) Screen for chemical modulators of autophagy reveals novel therapeutic inhibitors of mTORC1 signaling. *PLoS One 4*, e7124.

(48) Saiki, S., Sasazawa, Y., Imamichi, Y., Kawajiri, S., Fujimaki, T., Tanida, I., Kobayashi, H., Sato, F., Sato, S., Ishikawa, K., Imoto, M., and Hattori, N. (2011) Caffeine induces apoptosis by enhancement of autophagy via PI3K/Akt/mTOR/p70S6K inhibition. *Autophagy 7*, 176–187.

(49) Kawatani, M., Okumura, H., Honda, K., Kanoh, N., Muroi, M., Dohmae, N., Takami, M., Kitagawa, M., Futamura, Y., Imoto, M., and

Osada, H. (2008) The identification of an osteoclastogenesis inhibitor through the inhibition of glyoxalase I. *Proc. Natl. Acad. Sci. U.S.A. 105*, 11691–11696.

dx.doi.org/10.1021/cb200492h | *ACS Chem. Biol.* XXXX, XXX, XXX–XXX

The Journal of Antibiotics (2012) 65, 211–214

www.nature.com/ja

NOTE

Napyradiomycin A1, an inhibitor of mitochondrial complexes I and II

Kohta Yamamoto[1], Etsu Tashiro[1], Keiichiro Motohashi[2], Haruo Seto[2] and Masaya Imoto[1]

The Journal of Antibiotics (2012) **65,** 211–214; doi:10.1038/ja.2011.138; published online 18 January 2012

Keywords: mitochondrial electron transport; napyradiomycin; intracellular ATP level

We have previously proposed a cell-based screening method 'EGF-induced (epidermal growth factor) filopodium protrusion assay' to identify mitochondrial electron transport inhibitors or glycolysis inhibitors. Filopodia are spike-like cell membrane projections that contribute to tumor metastasis. Previously, we have reported that mitochondrial electron transport inhibition resulted in the inhibition of EGF-induced filopodium protrusion in human adenocarcinoma A431 cells only when their glycolytic pathways were restricted.[1] By using the inhibition of filopodium protrusion as an indicator, we identified napyradiomycin A1 (Figure 1a; isolated from *Streptomyces antimycoticus* NT17),[2] which was previously identified as an antibacterial antibiotic,[3] as a candidate of mitochondrial electron transport inhibitor. A431 cells were treated with napyradiomycin A1 with or without 10 mM 2-deoxy-D-glucose (Sigma-Aldrich, St Louis, MO, USA) for 30 min, followed by 30 ng ml^{-1} EGF (Sigma-Aldrich) stimulation and observation under a microscope. As shown in Figure 1b, 20 μM napyradiomycin A1 inhibited EGF-induced filopodium protrusion in A431 cells only in the presence of the glycolytic enzyme hexokinase inhibitor 2-deoxy-D-glucose. Mitochondrial electron transport inhibitor rotenone (Sigma-Aldrich) also inhibited filopodium protrusion only in the presence of 2-deoxy-D-glucose. Furthermore, it was reported that co-treatment with a mitochondrial electron transport inhibitor and a glycolytic inhibitor markedly decreased intracellular ATP levels.[1] We then tested whether napyradiomycin A1 decreased ATP levels in A431 cells in which glycolytic pathways were restricted. As intracellular ATP levels were not affected by EGF stimulation (data not shown), we measured intracellular ATP levels under the condition where A431 cells were treated with napyradiomycin A1 with or without 10 mM 2-deoxy-D-glucose for 30 min in the absence of EGF. After incubation, intracellular ATP levels were measured using a Cell Titer-Glo Luminescent Cell Viability Assay Kit (Promega, Madison, WI, USA) with a luminometer (Wallac; Perkin-Elmer, Waltham, MA, USA). As shown in Figure 1c, napyradiomycin A1 treatment did not decrease cellular ATP levels; however, 20 μM napyradiomycin A1 markedly decreased cellular ATP levels in the presence of 2-deoxy-D-glucose in A431 cells. Furthermore, ATP levels in HeLa cells also decreased under co-treatment with napyradiomycin A1 and 2-deoxy-D-glucose (data not shown). These results suggested that napyradiomycin A1 inhibited mitochondrial electron transport in cancer cells.

Next, we examined whether napyradiomycin A1 actually inhibited mitochondrial electron transport *in vitro* by using submitochondrial particles (SMP) obtained from the bovine heart. In order to prepare SMP, bovine hearts were homogenized in MSH buffer (210 mM mannitol, 70 mM sucrose, 1 mM DTT, 1 mM EGTA, 0.1% BSA and 10 mM HEPES pH 7.4) with a Potter-Elvehjem homogenizer (Nippon genetics, Tokyo, Japan). Homogenates were centrifuged at 1000 *g* for 10 min, and the resulting supernatant was further centrifuged at 8000 *g* for 20 min. Pellets were suspended in MSH buffer and obtained as SMP.[4]

The mitochondrial electron transport chain consists of four discrete multisubunit complexes: NADH–ubiquinone oxidoreductase (complex I), succinate–ubiquinone oxidoreductase (complex II), ubiquinol–cytochrome *c* oxidoreductase (complex III) and cytochrome *c* oxidase (complex IV). Therefore, we evaluated which complex was the target of napyradiomycin A1.

Mitochondrial complex I activity was measured by monitoring the absorbance change of NADH at 340 nm in the presence of antimycin A (Sigma-Aldrich) and KCN (Sigma-Aldrich), an inhibitor of complex III and complex IV, respectively.[5,6] The enzyme assay was performed at 30 °C in a buffer containing 50 mM phosphate (pH 7.4), 250 mM sucrose, 0.1 μg ml^{-1} antimycin A, 2 mM KCN, 50 μM decylubiquinone (DB; 2,3-dimethoxy-5-methyl-6-decyl-1,4-benzoquinone, an exogenous hydrophobic quinone that acts as electron acceptor; Sigma-Aldrich),[7] 0.2 mM NADH, and 12 μg ml^{-1} SMP with or without napyradiomycin A1. Rotenone was used as a positive control of complex I inhibitor. We found that napyradiomycin A1 inhibited complex I activity with an IC_{50} value of 20 μM (Figure 2a).

[1]Chemical Biology Laboratory, Department of Biosciences and Informatics, Faculty of Science and Technology, Keio University, Yokohama City, Japan and [2]Bioregulatory Laboratory, Faculty of Applied Biosciences, Tokyo University of Agriculture, Tokyo, Japan
Correspondence: Dr E Tashiro, Department of Biosciences and Informatics, Faculty of Science and Technology, Chemical Biology Laboratory, Faculty of Science and Technology, Keio University, 3-14-1 Hiyoshi, Kohoku-ku, Yokohama 223-8522, Japan.
E-mail: tashiro@bio.keio.ac.jp
Received 2 December 2011; revised 15 December 2011; accepted 16 December 2011; published online 18 January 2012

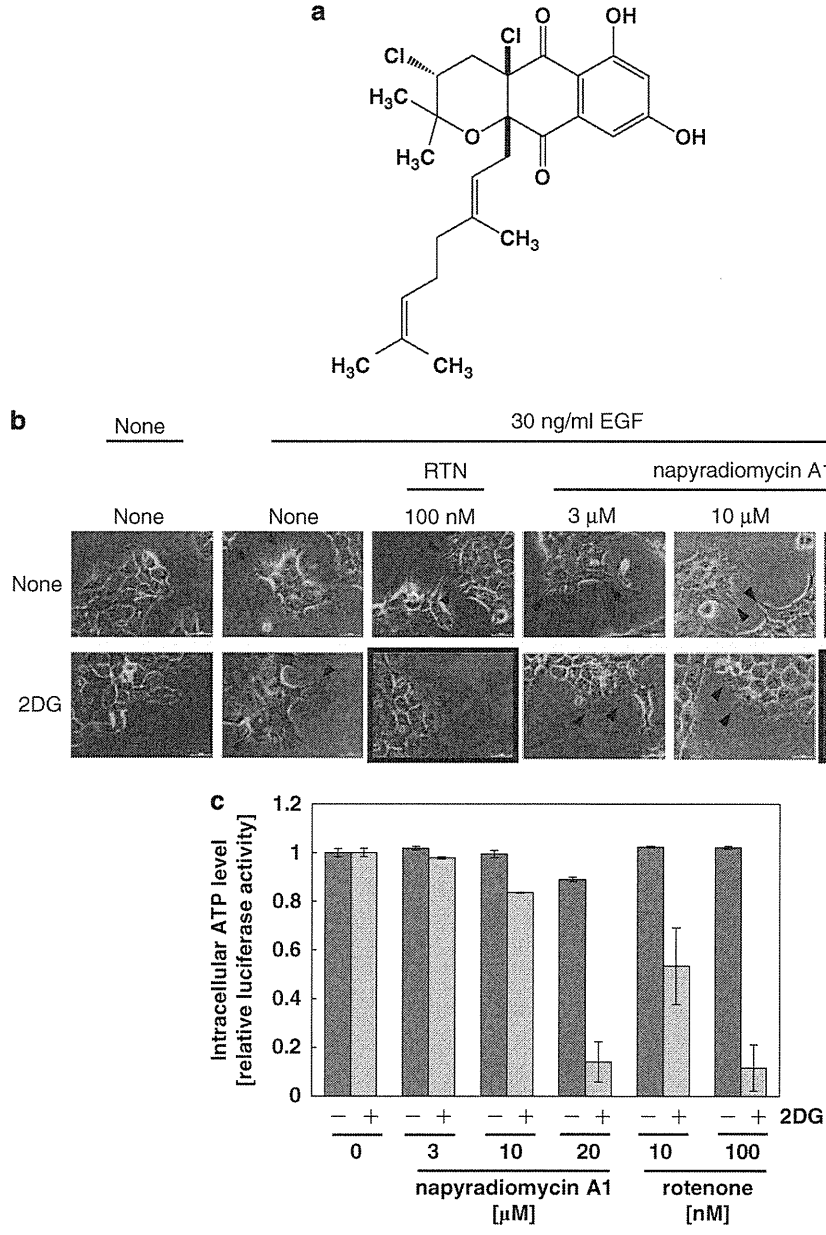

Figure 1 Napyradiomycin A1 decreased intracellular ATP levels. (**a**) The structure of napyradiomycin A1.[3] (**b**) Napyradiomycin A1 inhibited EGF-induced filopodia protrusion only in the presence of 2-deoxy-D-glucose (2DG, 10 mM). The assay method was as described previously.[1] Mitochondrial electron transport inhibitor rotenone (RTN 100 nM) was used as a positive control. Arrowhead indicates filopodia, and the framed photos show filopodium inhibition. (**c**) Napyradiomycin A1 decreased intracellular ATP levels in 2DG-treated A431 cells. A431 cells were treated with napyradiomycin A1 with or without 10 mM of 2DG for 30 min. After incubation, intracellular ATP levels were measured using a Cell Titer-Glo Luminescent Cell Viability Assay Kit with a luminometer.

Mitochondrial complex II activity was measured by monitoring the absorbance change of 2,6-dichlorophenolindophenol (Sigma-Aldrich) at 600 nm in the presence of rotenone and KCN.[8] The enzyme assay was performed at 30 °C in a buffer containing 50 mM phosphate (pH 7.4), 0.1 μM rotenone, 2 mM KCN, 40 μM 2,6-dichlorophenolindophenol, and 12 μg ml^{-1} SMP with or without napyradiomycin A1. Theonoyl trifluoroacetone (Sigma-Aldrich) was used as a positive control of complex II inhibitor.[9] We found that napyradiomycin A1 inhibited complex II activity with an IC_{50} value of 9.7 μM (Figure 2b).

Mitochondrial complex III activity was measured by monitoring the absorbance change of the reduction of oxidized cytochrome *c* at 550 nm in the presence of rotenone, KCN and an electron donor decylubiquinol. Decylubiquinol was obtained by the reduction of DB with sodium borohydride.[10] The enzyme assay was performed at 30 °C in a buffer containing 50 mM Tris (pH 7.6), 1 mM $MgCl_2$, 0.1 μM rotenone, 2 mM KCN, 40 μM cytochrome *c*, 50 μM decylubiquinol and 12 μg ml^{-1} SMP with or without napyradiomycin A1. Although antimycin A inhibited complex III activity, napyradiomycin A1 did not, even at 20 μM (Figure 2c)

Mitochondrial complex IV activity was measured by monitoring the absorbance change of the oxidation of reduced cytochrome *c* at 550 nm. The enzyme assay was performed at 30 °C in a buffer containing 50 mM Tris (pH 7.6), 1 mM $MgCl_2$, 0.1 μg ml^{-1} antimycin A, 0.1 μM rotenone, 20 μM reduced cytochrome *c* and 12 μg ml^{-1} SMP

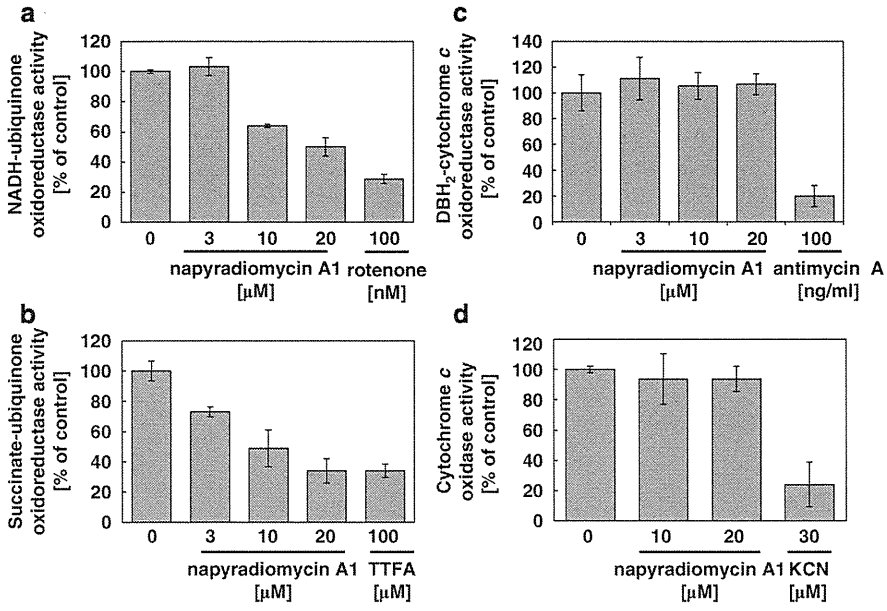

Figure 2 Napyradiomycin A1 inhibited mitochondrial complexes I and II. A modification of previously reported methods[10,16–18] was used to measure complex I, complex II, complex III and complex IV activities. (**a**) Napyradiomycin A1 inhibited complex I activity. Mitochondrial complex I (NADH–ubiquinone oxidoreductase) activity was measured by monitoring the absorbance change of NADH at 340 nm using SMP. (**b**) Napyradiomycin A1 inhibited complex II activity. Mitochondrial complex II (Succinate–ubiquinone oxidoreductase) activity was measured by monitoring the absorbance change of 2,6-dichlorophenolindophenol at 600 nm using SMP. (**c**) Napyradiomycin A1 did not inhibit complex III activity. Mitochondrial complex III (decylubiquinol (DBH_2)–cytochrome *c* oxidoreductase) activity was measured by monitoring the absorbance change of cytochrome *c* at 550 nm using SMP. (**d**) Napyradiomycin A1 did not inhibit complex IV activity. Mitochondrial complex IV (cytochrome *c* oxidase) activity was measured by monitoring the absorbance change of the oxidation of reduced cytochrome *c* at 550 nm using SMP. SMP were obtained by standard different centrifugation.[4] All data are the mean ± s.d. of three independent experiments.

with or without napyradiomycin A1. Although KCN inhibited complex IV activity, 20 μM napyradiomycin A1 inhibited complex IV activity less than 10% (Figure 2d).

In conclusion, napyradiomycin A1 inhibited mitochondrial complexes I and II, but did not inhibit complex III or IV *in vitro*. Therefore, it was suggested that mitochondrial electron transport inhibition by napyradiomycin A1 was caused by the inhibition of mitochondrial complexes I and II.

It was reported that the isoprenyl unit of ubiquinone was important to bind to mitochondrial complex I.[11] It has been also reported that two isoprene units of ubiquinone could be modeled in the native structure of complex II by computational analysis using a protein-ligand docking program.[12] Napyradiomycin A1 is structurally similar to ubiquinone (Figure 1a); therefore, it is likely that napyradiomycin A1 binds with the ubiquinone-binding site of complexes I and II through its terpenoid residue. On the other hand, although mitochondrial complex III also includes a ubiquinone-binding site,[13] napyradiomycin A1 was unable to inhibit the activity of complex III up to 20 μM. Our result that napyradiomycin A1 inhibits mitochondrial complexes I and II but not complex III is interesting, because it has been reported that the structure of ubiquinone-binding sites in complex I and complex III may be similar, but they are different from a ubiquinone-binding site in complex II.[14] Further study is necessary to elucidate the mechanism by which napyradiomycin A1 inhibits mitochondrial complexes I and II but not complex III.

Isolation of napyradiomycins was first reported in 1986. Napyradiomycin group compounds were isolated from *Actinomycetes* and identified as antibacterial antibiotics.[3] At present, many napyradiomycins have been identified and reported to exhibit cytotoxicity against human cancer cell lines;[15] however, the molecular mechanism by which napyradiomycins show cytotoxicity has been unclear. Our results raise the possibility that an inhibitory effect of napyradiomycin A1 against the mitochondrial electron transport chain may explain the cytotoxicity of napyradiomycins against cancer cells.

ACKNOWLEDGEMENTS

This study was partly supported by a Grant-in-Aid for Scientific Research from the Ministry of Education, Culture, Sports, Science and Technology of Japan. This study was also supported by grants from Suzuken Memorial Foundation. This study was supported in part by the Global COE Program for Human Metabolomic Systems Biology of MEXT, Japan.

1 Kitagawa, M., Ikeda, S., Tashiro, E., Soga, T. & Imoto, M. Metabolomic identification of the target of the filopodia protrusion inhibitor glucopiericidin A. *Chem. Biol.* **17,** 989–998 (2010).
2 Motohashi, K., Sue, M., Furihata, K., Ito, S. & Seto, H. Terpenoids Produced by Actinomycetes: Napyradiomycins from Streptomyces antimycoticus NT17. *J. Nat. Prod.* **71,** 595–601 (2008).
3 Shiomi, K. *et al.* Novel antibiotics napyradiomycins. Production, isolation, physicochemical properties and biological activity. *J. Antibiot.* **39,** 487–493 (1986).
4 Pedersen, P L. *et al.* Preparation and characterization of mitochondria and submitochondrial particles of rat liver and liver-derived tissues. *Methods Cell Biol.* **20,** 411–481 (1978).
5 di Rago, J P. & Colson, A M. Molecular basis for resistance to antimycin and diuron, Q-cycle inhibitors acting at the Q_i site in the mitochondrial ubiquinol-cytochrome c reductase in *Saccharomyces cerevisiae*. *J. Biol. Chem.* **263,** 12564–12570 (1988).
6 Chance, B. The kinetics and inhibition of cytochrome components of the succinic oxidase system. III. Cytochrome b. *J. Biol. Chem.* **233,** 1223–1229 (1958).
7 Lenaz, G. *et al.* Coenzyme Q deficiency in mitochondria: kinetic saturation versus physical saturation. *Mol. Aspects Med.* **18**(Suppl), S25–31 (1997).
8 Chance, B., Williams, G R. & Hollunger, G. Inhibition of electron and energy transfer in mitochondria. I. Effects of Amytal, thiopental, rotenone, progesterone, and methylene glycol. *J. Biol. Chem.* **238,** 418–431 (1963).

9 Paddenberg, R. *et al.* Essential role of complex II of the respiratory chain in hypoxia-induced ROS generation in the pulmonary vasculature. *Am. J. Physiol. Lung Cell Mol. Physiol.* **284,** L710–719 (2003).
10 Rhein, V. *et al.* Amyloid-beta leads to impaired cellular respiration, energy production and mitochondrial electron chain complex activities in human neuroblastoma cells. *Cell Mol. Neurobiol.* **29,** 1063–1071 (2009).
11 Warncke, K. *et al.* Influence of hydrocarbon tail structure on quinone binding and electron-transfer performance at the Q_A and Q_B sites of the photosynthetic reaction center protein. *Biochemistry* **33,** 7830–7841 (1994).
12 Horsefield, R. *et al.* Structural and computational analysis of the quinone-binding site of complex II (succinate-ubiquinone oxidoreductase): a mechanism of electron transfer and proton conduction during ubiquinone reduction. *J. Biol. Chem.* **281,** 7309–7316 (2006).
13 Xia, D. *et al.* Crystal structure of the cytochrome bc_1 complex from bovine heart mitochondria. *Science* **277,** 60–66 (1997).
14 Tan, A. K., Ramsay, R. R., Singer, T. P. & Miyoshi, H. Comparison of the structures of the quinone-binding sites in beef heart mitochondria. *J. Biol. Chem.* **268,** 19328–19333 (1993).
15 Soria-Mercado, I. E., Prieto-Davo, A., Jensen, P. R. & Fenical, W. Antibiotic terpenoid chloro-dihydroquinones from a new marine actinomycete. *J. Nat. Prod.* **68,** 904–910 (2005).
16 Brusque, A. M. *et al.* Inhibition of the mitochondrial respiratory chain complex activities in rat cerebral cortex by methylmalonic acid. *Neurochem. Int.* **40,** 593–601 (2002).
17 Telford, J. E., Kilbride, S. M. & Davey, G. P. Decylubiquinone increases mitochondrial function in synaptosomes. *J. Biol. Chem.* **285,** 8639–8645 (2010).
18 Silveira, P. C., Streck, E. L. & Pinho, R. A. Evaluation of mitochondrial respiratory chain activity in wound healing by low-level laser therapy. *J. Photochem. Photobiol. B* **86,** 279–282 (2007).

Antitumor effects of novel highly hydrophilic and non-ATP-competitive MEK1/2 inhibitor, SMK-17

Masaki Kiga[a,c], Fumie Tanzawa[a], Shiho Iwasaki[a], Fumi Inaba[a], Kosaku Fujiwara[a], Hayato Iwadare[a], Tomoki Echigo[a], Yuji Nakamura[b], Tomoyuki Shibata[b], Kanae Suzuki[b], Isao Yasumatsu[a], Ayako Nakayama[c], Yukiko Sasazawa[c], Etsu Tashiro[c], Masaya Imoto[c] and Shinichi Kurakata[b]

The mitogen-activated protein kinase (MAPK) signal pathway plays a central role in regulating tumor cell proliferation, survival, and differentiation. The components of this pathway, Ras/Raf/MEK/ERK, are frequently activated in human cancers. Targeting this pathway is considered to be a promising anticancer strategy. In particular, MEK is an attractive drug target because of its high selectivity to ERK. We can expect potent growth inhibitory and proapoptotic effects by inhibiting MEK. Here, we report derivatives of *N*-[2-(2-chloro-4-iodo-phenylamino)-3,4-difluorophenyl]-methanesulfonamide as novel MEK1/2 inhibitors. Among these compounds, we found SMK-17 to be a potent MEK1/2 inhibitor with high aqueous solubility. The in-silico docking study suggested that SMK-17 is bound to an allosteric pocket of MEK1. The kinetic study and the kinase profiler analysis confirmed the allosteric nature of SMK-17. SMK-17 inhibited MEK1 kinase activity in a non-ATP-competitive manner and it was highly selective to MEK1 and 2. SMK-17 inhibited the growth of tumor cell lines *in vitro*. Especially, it seemed that cell lines harboring highly phosphorylated MEK1/2 and ERK1/2 were highly sensitive to SMK-17. Moreover, unlike previously reported MEK inhibitors, PD184352 or U0126, SMK-17 did not inhibit the phosphorylation of ERK5. *In vivo*, SMK-17 exhibited potent antitumor activity in animal models on oral administration. SMK-17 selectively blocked the MAPK pathway signaling without affecting other signal pathways, which resulted in significant antitumor efficacy without notable side effects. These findings suggest that SMK-17, an exquisitely selective, orally available MEK1/2 inhibitor, is a useful chemical biology tool for characterizing the function of MEK/MAPK signaling both *in vitro* and *in vivo*. *Anti-Cancer Drugs* 23:119–130 © 2011 Wolters Kluwer Health | Lippincott Williams & Wilkins.

Anti-Cancer Drugs 2012, 23:119–130

Keywords: allosteric inhibition, antitumor activities, cell cycle arrest, kinase inhibitor, xenograft model

[a]Kasai R&D Center, [b]Shinagawa R&D Center, Daiichi Sankyo Co. Ltd, Tokyo and [c]Department of Biosciences and Informatics, Faculty of Science and Technology, Keio University, Yokohama, Japan

Correspondence to Masaki Kiga and Kosaku Fujiwara, Kasai R&D Center, Daiichi Sankyo, Co. Ltd, 1-16-13, Kitakasai, Edogawa-ku, Tokyo 134-8630, Japan
Tel: +81 336 800 151; fax: +81 356 964 264;
e-mail: kiga.masaki.sm@daiichisankyo.co.jp and
fujiwara.kosaku.t2@daiichisankyo.co.jp

Received 20 May 2011 Revised form accepted 27 August 2011

Introduction

The mitogen-activated protein kinases (MAPKs) are a family of serine/threonine protein kinases that play an important role in many cellular responses such as cell proliferation, survival, differentiation, movement, and apoptosis. The extracellular signal-regulated kinases 1 and 2 (ERK1/2) are the first characterized members of the MAPK family. ERK1/2 are activated by a phosphorylation cascade, downstream from the receptor tyrosine kinases, the ras protooncogene, Raf, and MEK1/2. Activated MEK1/2 catalyzes the phosphorylation of ERK1/2. These MAPKs phosphorylate a variety of substrates, including p90RSK and the transcription factor Elk-1, which mainly promote cell growth [1,2]. MEK1/2, also known as MKK1/2, are members of a large family of dual-specificity kinases (MKK1–7) that phosphorylate threonine and tyrosine residues of various MAPKs. Thus far, the only known substrates of MEK1/2 are ERK1/2. This tight selectivity indicates that MEK1/2 are essential for the MAPK pathway.

Constant activation of the MAPK pathway, because of aberrant receptor tyrosine kinase activation and Ras or BRAF mutations, is found frequently in human cancers and represents a major factor in determining abnormal cell growth [3]. Approximately 30% of all human cancers contain an activating Ras mutation. The incidence of K-ras mutations is particularly high in pancreatic and colon cancers (90 and 44%, respectively) [4]. Oncogenic V600E mutations in BRAF have been found in 66% of melanomas and 69% of papillary thyroid cancers [5,6]. Furthermore, aberrant activation of the MAPK pathway correlates with tumor progression and poor prognosis in patients with various cancers. Although active mutations of MEK1/2 have not been found in human cancers, the constitutive expression of MEK1/2 is sufficient to induce transformation [7,8]. Targeting MEK1/2 with a small

All supplementary digital content is available directly from the corresponding author.

0959-4973 © 2011 Wolters Kluwer Health | Lippincott Williams & Wilkins

DOI: 10.1097/CAD.0b013e32834c6a33

molecule inhibitor is an attractive strategy because of the potential to prevent all upstream aberrant oncogenic signaling [9,10]. Although previously reported MEK inhibitors, PD184352/CI-1040 and PD0325901, have been evaluated in a clinical study, these clinical trials were discontinued because of insufficient efficacy and undesirable adverse events [11–14]. ARRY142886/AZD6244 has been evaluated for clinical proof-of-concept in clinical trials. This compound has shown clinical responses in some patients with malignant melanoma and thyroid carcinoma [14,15]. However, no MEK inhibitors have been approved in the clinical use yet. More effective MEK inhibitors than previously reported compounds are needed for cancer therapy.

We report that SMK-17 is a hydrophilic, highly selective, and potent MEK1/2 inhibitor with a distinctively structured, piperidine sulfamide scaffold. SMK-17 exhibits significant antitumor activity *in vitro* and *in vivo* by selectively blocking the MAPK pathway signaling.

Materials and methods

Compounds

All compounds shown in Tables 1 and 2 were synthesized in-house, according to the procedure described in the patent application (WO2004083167).

Cell-free kinase assay

Homogeneous time-resolved fluorescence (HTRF) was used to detect MEK1/2 kinase activity. The reagents used in the assay are described below. Recombinant active human MEK1, MEK2, and GST-fused ERK2 were purchased from Millipore (Bedford, Massachusetts, USA). ATP was from Sigma-Aldrich Chemical (Saint Louis, Missouri, USA). Anti-phospho-ERK1/2 polyclonal antibody #9101 was from Cell Signaling Technology (Danvers, Massachusetts, USA). Polyclonal goat anti-rabbit antibody labeled with europium cryptate (PAR-K) and monoclonal anti-GST antibody labeled with XL665 (Mab GST-XL) were from Cisbio Bioassays (Bedford, Massachusetts, USA). In the presence or absence of testing compounds, the kinase reaction was conducted in 50 µl of reaction buffer [Tris (50 mmol/l), pH 7.4, $MgCl_2$ (10 mmol/l), EGTA (2 mmol/l), Na_3VO_4 (1 mmol/l), BSA (1 mg/ml)] containing 100 µmol/l ATP in a usual assay, 24 ng of active MEK1 or MEK2, and 100 ng of GST-fused ERK2 on a 96-well half-area EIA/RIA plate (Corning, New York, USA). After incubation at 30°C for 30 min, 25 µl of detection buffer [KF (1 mol/l), EDTA-PBS (50 mmol/l)], containing 1/500 diluted PAR-K, 1/1000 diluted antiphospho ERK1/2 polyclonal antibody, and 1/250 diluted MAb GST-XL, was added. After overnight incubation with a detection buffer, the phosphorylated ERK2 was measured with the Discovery HTRF microplate analyzer (PerkinElmer, Waltham, Massachusetts, USA). A ratio of 665 nm signal to 620 nm signal was regarded as the quantum of phosphorylation of ERK2. Values of wells that did not contain MEK were used as the baseline in each plate. IC_{50} (50% inhibitory concentration) values of MEK inhibition were calculated using the curve-fitting GraphPad Prism version 4 (GraphPad software, La Jolla, California, USA) from triplicate sets of data.

Table 1 Identification of a sulfamide compound as an MEK inhibitor

Compound		MEK1 kinase IC_{50} (nmol/l)	pERK in cell EC_{50} (nmol/l)	*c*Log $D_{7.4}$	Solubilities JP-1/JP-2 (nmol/l)
1	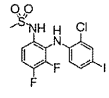	670	180	3.95	1.0/<0.5
PD184352	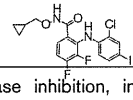	33	79	6.77	<0.5/<0.5

MEK1 kinase inhibition, intracellular MEK inhibition, *c*Log *D*, and aqueous solubility assay results of compound 1 and PD184352 as a reference compound.

Kinase selectivity

Kinase selectivity of SMK-17 at 1 µmol/l was tested against 233 human kinases by the Kinase Profiler (Millipore, *http://www.millipore.com/life_sciences/flx4/lld_kinases&tab1=3#tab1=3:tab2=1*).

Physicochemical study

JP-1 (aqueous acidic solution, pH 1.2) and JP-2 (neutral pH solution, pH 6.8) were purchased from Kanto Chemical (Tokyo, Japan). The sample solution was assayed using high-performance liquid chromatography (HPLC) methodologies. Two hundred and fifty micromoles per liter of the compound in aqueous CH_3CN solution [1 : 1 (v/v)] was prepared to make a calibration curve. The solubility was determined by comparing the ultraviolet peak area of the standard solution. The *c*Log *D* values were calculated by CLOGP software version 4.8.2 (Daylight Chemical Information Systems, Laguna Niguel, California, USA).

In-silico docking study

The molecular docking study was performed using Glide version 5.5 (Schrödinger, New York, New York, USA). The inhibitor was docked flexibly to an allosteric pocket adjacent to the ATP binding site of MEK1. The coordinates for the MEK1 were taken from a Protein Data Bank (PDBID: 3E8N [16]). In this structure, an allosteric inhibitor is bound adjacent to the ATP. The inhibitor molecule and water molecules that are unlikely to be important for ligand binding were deleted. Four structural water molecules that were bound to the magnesium ion or the side chain of A208 in the catalytic site, or the phosphates of the ATP, were preserved. After docking SMK-17 into the MEK1, energy minimization

Table 2 The structure–activity relationship of piperidine sulfamide scaffold for MEK inhibition and solubility screening

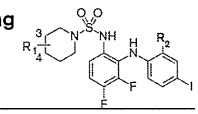

Piperidine series							
Compound	Substitution position	R1	R2	MEK1 kinase IC_{50} (nmol/l)	pERK in cell EC_{50} (nmol/l)	*c*Log $D_{7.4}$	Solubilities JP-1/JP-2 (nmol/l)
2	3-		Cl	40	360	3.42	-/-
3			F	42	770	−0.22	100/86
4			F	270	1500	−0.09	87/77
5			F	50	530	−0.41	91/88
6			F	34	110	−0.61	91/86
7	4-		Me	260	900	2.92	-/-
8			F	210	1500	2.45	12/21
9			Cl	210	400	3.39	-/-
10			Cl	180	300	3.68	1/2
11			Me	290	1800	−0.19	87/80
12			F	60	150	−0.65	92/84
13			Cl	92	52	0.73	88/74
14			Cl	74	800	0.63	89/61
15			Cl	72	190	0.71	-/-
16			F	33	220	−0.33	74/90
17 (SMK-17)			Cl	62	50	0.59	91/77
18			Cl	20	210	0.95	-/-
19			F	14	130	−0.31	86/78
20			F	41	430	−0.71	-/-
21			Cl	210	46	3.64	3/1

All tests were conducted by the same methods as in Table 1.

was performed on the complex with MacroModel version 9.7 (Schrödinger).

Cell culture

Colon 26 cells were provided by the Institute of Development, Aging, and Cancer, Tohoku University (Sendai, Japan). Other cell lines used in the experiments were purchased from American Type Culture Collection, and they were maintained with the recommended media supplemented with 10% heat-inactivated fetal bovine serum (HyClone Laboratories, Thermo Fisher Scientific, Waltham, Massachusetts, USA).

Western blot analysis

Anti-phospho-ERK (T202/Y204), anti-phospho-MEK (S217/221), anti-MEK1, anti-MEK2, anti-phospho-AKT (S473), anti-AKT, anti-cyclin D1, anti-phospho-S6 ribosomal protein (S235/236), anti-S6 ribosomal protein, anti-phospho-ERK5 (T218/Y220), anti-ERK5, anti-phospho-JNK (T183/Y185), anti-JNK, anti-phospho-p38 (T180/Y182), anti-p38α, anti-mouse HRP-linked IgG (#7076), and anti-rabbit HRP-linked IgG (#7074) were from Cell Signaling Technology. PhosphoSTOP; phosphatase inhibitor cocktail tablets and Complete Mini; and protease inhibitor cocktail tablets were from Roche Diagnostics (Indianapolis, Indiana, USA). Cells were seeded in six-well plates (Corning) 1 day before compound treatment. Then, the cells were treated with the compound for a specified period of time. Cells were harvested and lysed immediately with RIPA buffer (Tris HCl (50 mmol/l), pH 7.5, NaCl (150 mmol/l), Na_3VO_4 (1 mmol/l), 0.l% SDS, 0.5% deoxycholic acid, 1% IGEPAL CA-630, Phospho-

Fig. 1

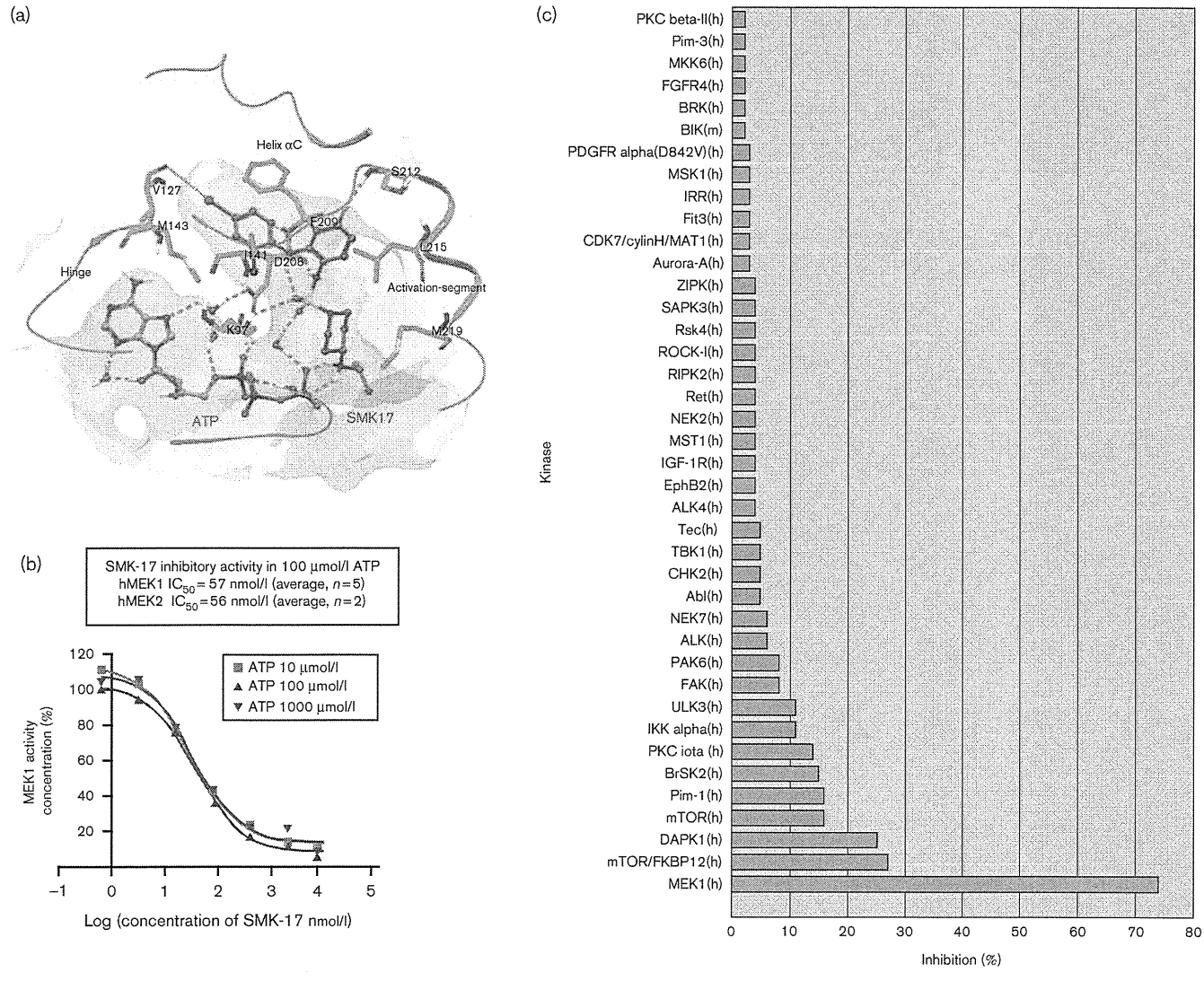

MEK1 kinase inhibition by SMK-17. (a) The predicted binding mode of SMK-17 with MEK1. View from the N-lobe. For simplicity, only important residues are shown. The hydrogen bondings and salt bridges are represented by cyan dotted lines. The MEK1 pocket surface is shown as a transparent gray surface. The figure was generated using Maestro version 9.0. (b) MEK kinase inhibition by SMK-17 at various ATP concentrations. Phosphorylation of ERK2 induced by MEK1 was detected by the homogeneous time-resolved fluorescence method. The IC_{50} value for MEK1 inhibition in this assay with 100 μmol/l of ATP was 37 nmol/l. The mean value of several independent experiments was 57 nmol/l for MEK1 kinase inhibition ($n=5$) and 56 nmol/l for MEK2 ($n=2$). (c) The Millipore Kinase Profiler data on 233 human kinases indicated that SMK-17 is a selective inhibitor against hMEK1 (1000 nmol/l, approximately 18-fold higher than IC_{50} for MEK1). The *x*-axis shows the percentage of inhibition against a specific kinase (*y*-axis). The top 40 kinases are shown in this figure.

STOP tablet, and Complete Mini tablet). Tumor tissues were harvested from mice and stored at −80°C and disrupted by grinding for 30 s at 2500 r.p.m. twice with a Multi-Beads Shocker (Yasui Kikai, Shizuoka, Japan) in the RIPA buffer. After incubation on ice for 30 min, the lysates were centrifuged at 14 000 *g* for 15 min to clear the insoluble fragments. The supernatants were used for western blot analysis. Equal amounts of total protein were resolved on SDS-PAGE gels and blotted with antibodies as indicated. The chemiluminescent signal was generated with Western Lightning Plus (PerkinElmer) and detected with a LAS-4000 imager (Fujifilm, Tokyo, Japan). The densitometric quantification of specific bands was performed using Multi Gauge Software (Fujifilm).

Cell enzyme-linked immunosorbent assay

NIH 3T3 cells were seeded at the appropriate density (1×10^5 cells/ml/well) on a 24-well flat-bottomed plate (Corning) and cultured for 24 h. The culture medium was changed to Dulbecco's Modified Eagle's Medium supplemented with 0.2% FBS. After 24 h incubation, the cells were treated with the compound for 1 h. Then,

Fig. 2

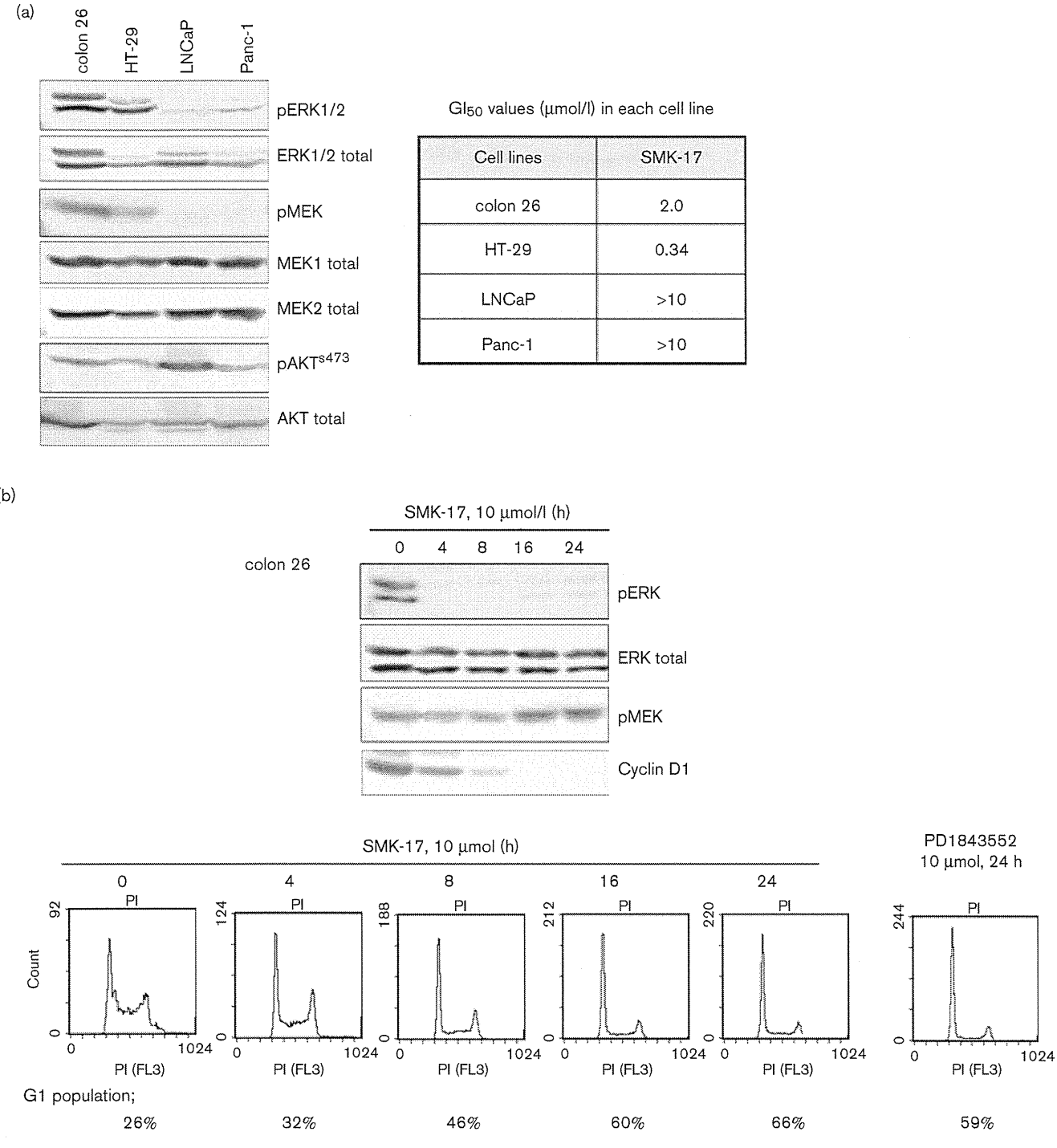

GI_{50} values (μmol/l) in each cell line

Cell lines	SMK-17
colon 26	2.0
HT-29	0.34
LNCaP	>10
Panc-1	>10

Growth inhibition profile of SMK-17. (a) Expression profile of MEK and ERK. Western blot analysis for pERK, ERK, pMEK, MEK1/2, pAKT^{S473}, and AKT. GI_{50} values of SMK-17 in a 72-h ATP assay are shown. (b–d) Effects of SMK-17 on the cell cycle and MEK/ERK pathway proteins in colon 26 (b), HT-29 (c), and Panc-1 (d). SMK-17-induced and PD184352-induced G1 cell cycle arrest in colon 26 and HT-29 cells. Colon 26, HT-29, and Panc-1 cells were treated with SMK-17 (1, 10, or 30 μmol/l respectively; three-fold to five-fold of GI_{50} for each cell line) or PD184352 for 24 h and the cell cycle profiles were examined by flow cytometry analysis. The values for cell cycle distribution were derived using MultiCycle software. SMK-17 affects the expressions of proteins that are critical to G1 phase transition in the cell cycle. Cells were treated with SMK-17 for 24 h, and the cell lysates were analyzed by western blot using antibodies as indicated. (e) Dose correlation between MEK inhibition and cell cycle arrest on HT-29 cells. Phosphorylation and the total ERK expression after 24-h drug treatment were evaluated with a western blot. The G1 phase population was examined by flow cytometry analysis.

Fig. 2 (continued)

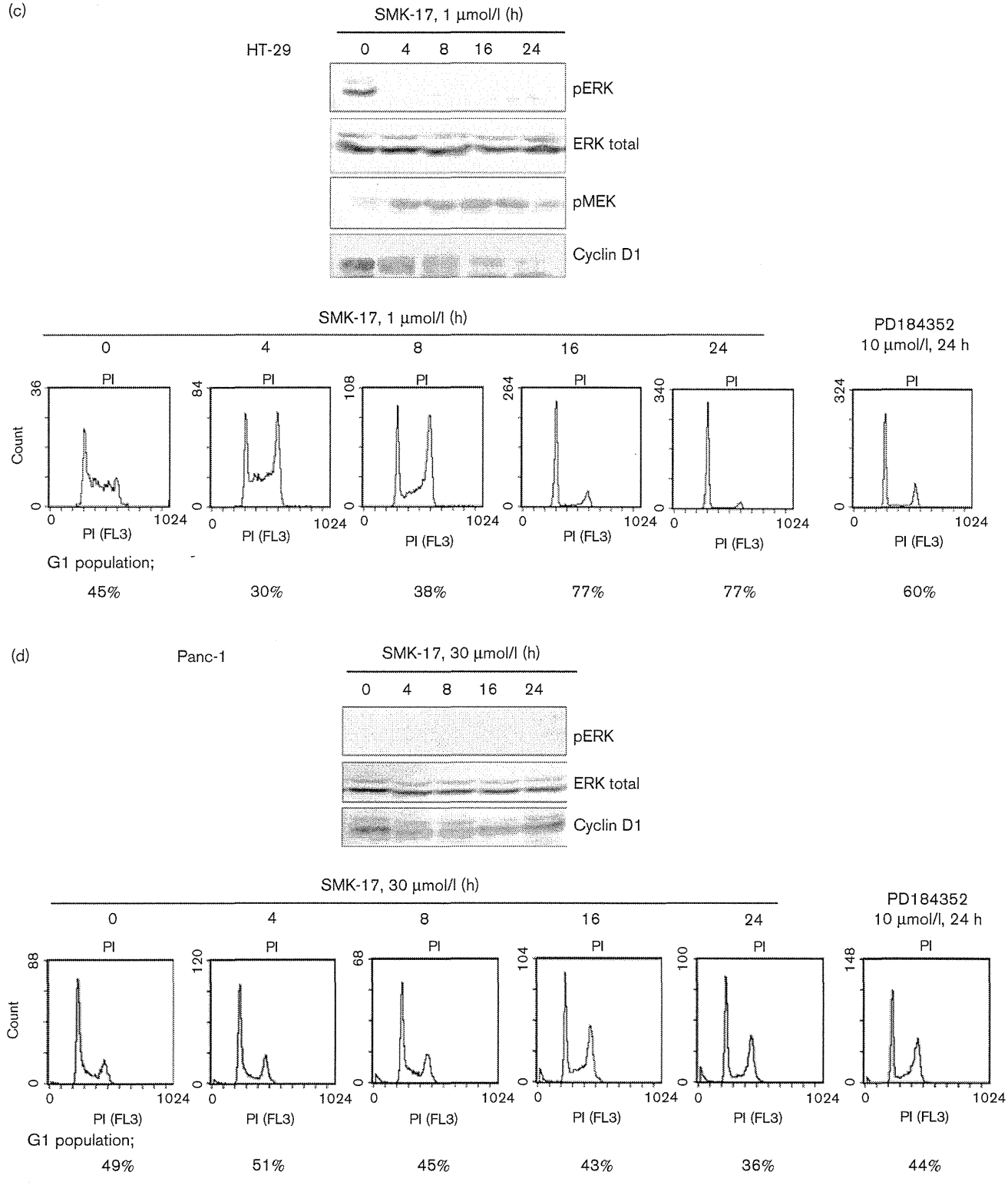

Fig. 2 (continued)

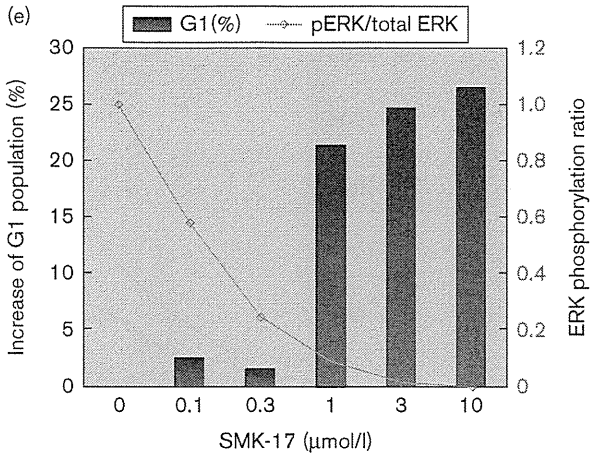

the cells were stimulated with an epidermal growth factor (EGF; Calbiochem, Merck KGaA, Darmstadt, Germany, final concentration 10 ng/ml) for 5 min. The cells were washed with cold PBS containing Na_3VO_4 (1 mmol/l) and fixed with −20°C methanol for 5 min. The cells were treated with blocking buffer (1% BSA, 0.05% Tween20-PBS) for 1 h, and incubated with primary antibodies for 2 h at 4°C. After being washed with 0.05%-Tween20-PBS twice, HRP-linked secondary antibodies in 1/1000 dilution was added and incubated at 4°C for 1 h. The cells were then washed three times and the detection substrate was added (OPD coloring reaction kit from Sumitomo Bakelite, Tokyo, Japan). The absorbance at 490 nm was then measured with a microplate reader (Model 3550, Bio-Rad Laboratories, Hercules, California, USA). In this experiment, EC_{50} values of MEK inhibition were calculated using the linear regression method. Two concentrations of each compound, which yielded MEK inhibitions closest to 50%, were chosen to calculate the EC_{50} values.

Cell growth inhibition assays

For growth inhibition experiments, cells were plated in black 96-well plates (Corning) at 1000 cells/100 μl/well. After 24-h culture, the compound was added and incubated for another 72 h. The cell number was measured using CellTiter-Glo (Promega, Fitchburg, Wisconsin, USA). Nonlinear curve fitting was performed using GraphPad Prism 4 from triplicate sets of data.

Cell cycle measurement

The percentage of cells in different cell cycle phases of division was measured by flow cytometry using propidium iodide (PI, Sigma-Aldrich) staining of cells [17]. In brief, tumor cells were treated with SMK-17 for the indicated time, fixed with 70% ethanol at −20°C, and then stained with PI (40 μg/ml) and RNase A (0.5 mg/ml) (Wako Pure Chemical Industries, Osaka, Japan) at 37°C for 30 min. PI fluorescence was measured with an EPICS XL Flow Cytometer (Beckman Coulter, Brea, California, USA) and analyzed using MultiCycle software (Phoenix Flow Systems, San Diego, California, USA)

Pharmacokinetic studies

SMK-17 was dosed by oral gavage to tumor-bearing mice. Three mice of each group were sacrificed after dosing, and plasma samples were collected and frozen at −20°C until analysis.

Acetonitrile deproteinized the plasma samples with a two-fold volume of the sample. The supernatant was obtained by centrifugation at 15 000*g* for 3 min at 4°C. Plasma concentrations of SMK-17 were determined by high-performance liquid chromatography analysis with ultraviolet detection at 280 nm. The mobile phase of HPLC was 0.5% phosphoric acid/acetonitrile (57/43, v/v) and the flow-rate was 1 ml/min through a YMC-Pack ODS-A column (A-312, 150 × 6.0 mm I.D., S-5 μm, YMC, Kyoto, Japan).

In-vivo antitumor study

Specific pathogen-free female nude mice (BALB/cA Jcl-nu) were purchased from CLEA Japan (Tokyo, Japan). Female CDF1 mice were from Charles River Japan (Yokohama, Japan). SMK-17 and PD184352 were suspended in 0.5% methyl cellulose solution (Wako Pure Chemical Industries), and administered daily to the animals by gavage (0.1 ml/10 g body weight). Control animals received 0.5% methyl cellulose solution for vehicle control. For the HT-29 study, 2×10^6 tumor cells were inoculated subcutaneously into the axillar region of the nude mice on Day 0. Tumor-bearing nude mice were grouped, and administration of SMK-17 or PD184352 was started on Day 3. For the colon 26 study, 2×10^5 cells were inoculated subcutaneously into CDF1 mice on Day 0. Tumor-bearing mice were grouped, and drug treatment was started on Day 3. Tumor volumes were calculated using a microgauge (Mitsutoyo, Kawasaki, Japan) according to the following equation: Tumor volume (mm^3) = $1/2 \times (\text{tumor length}) \times (\text{tumor width})^2$.

Results and discussion

Potency of diphenyl amine sulfonamide derivatives as an MEK1/2 inhibitor

In this article, we describe the discovery of the new derivative series of diphenyl amine sulfonamide as potent MEK inhibitors. We summarize the optimization of the sulfonamide modification, which has culminated in the identification of the potent and highly water soluble MEK inhibitor, SMK-17 (compound 17 in Table 2). The goal of this study was to identify a compound that possessed potent antitumor activity *in vivo* with high oral availability, which required high aqueous solubility for oral absorption and a strong MEK-inhibiting activity. An HTRF-based kinase assay was used for the primary screening. Then, phospho-ERK-detecting cell enzyme-

Fig. 3

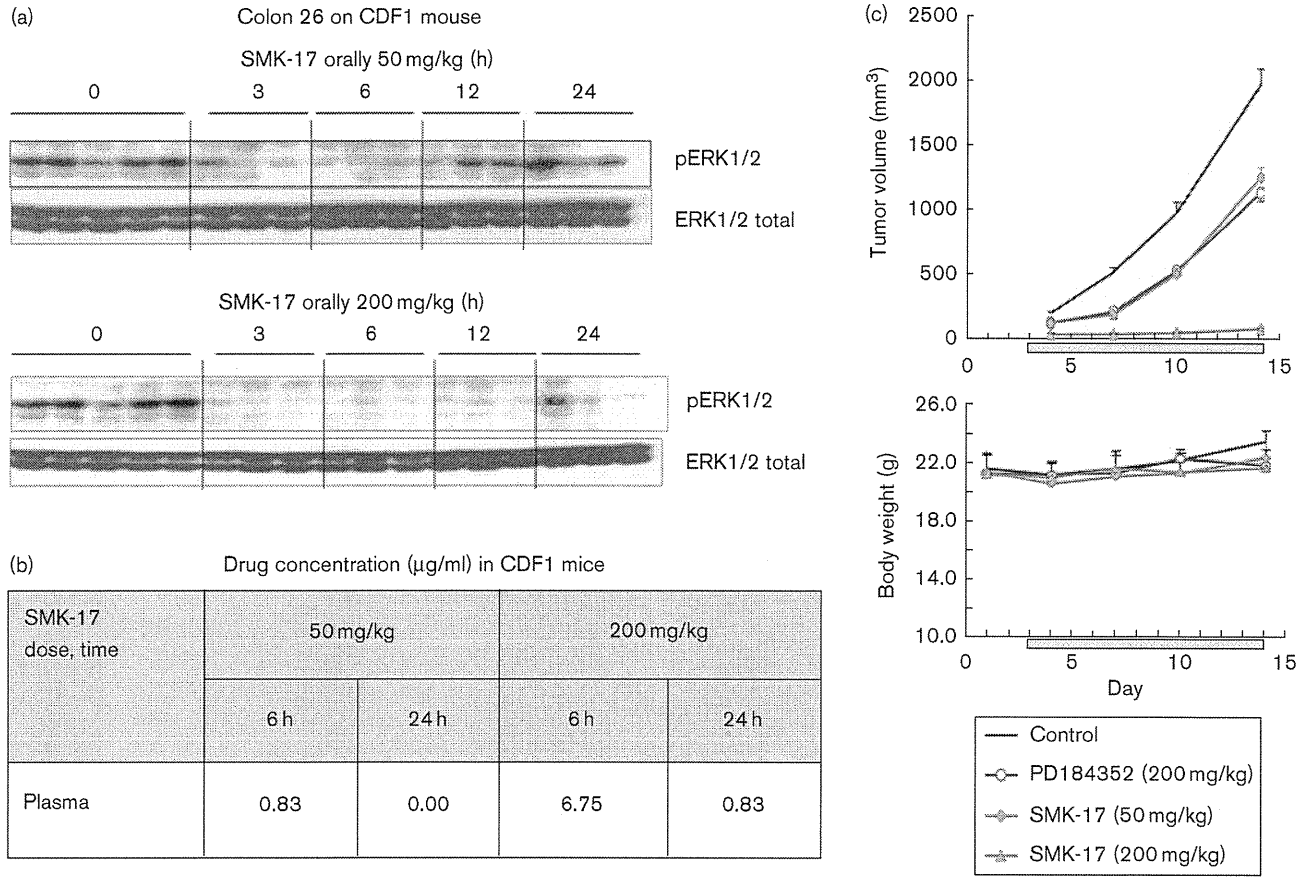

(b) Drug concentration (μg/ml) in CDF1 mice

SMK-17 dose, time	50 mg/kg		200 mg/kg	
	6 h	24 h	6 h	24 h
Plasma	0.83	0.00	6.75	0.83

The *in-vivo* efficacy of SMK-17. (a) After a single oral dose of SMK-17 to colon 26-CDF1 mice, tumors were excised at various time points after dosing, and the tumor lysates were analyzed by western blot. Administration of SMK-17 at 50 mg/kg achieved phospho-ERK1/2 inhibition in tumors for 6 h. Significant phospho-ERK1/2 inhibition was observed up to 24 h after dosing in mice treated with 200 mg/kg compared with the untreated controls. (b) SMK-17 concentration (μg/ml) in the plasma of the drug-treated CDF1 mice after administration. (c) SMK-17 exhibits significant in-vivo antitumor efficacy that correlates with its inhibition of MAPK signaling in colon26-CDF1 mice. (d) Western blot analysis of MAPKs and AKT signals in an HT-29 xenograft. (e) In-vivo antitumor activity of SMK-17 on HT-29 xenograft.

linked immunosorbent assay was used to measure the intracellular MEK activity. The oral absorption of each compound was predicted by calculating the lipophilicity ($c\,Log\,D$) and aqueous solubility.

We identified a novel compound, *N*-[2-(2-chloro-4-iodo-phenylamino)-3,4-difluorophenyl]-methanesulfonamide (compound 1 in Table 1), as an MEK inhibitor in the above-described screening. It has a sulfamide substituent that is different from previously reported MEK inhibitors such as U0126, PD98059, and PD184352. This compound showed weak activity in in-vitro assays and poor water solubility: less than 0.5 μmol/l of solubility in pH 6.8 solution. We adopted compound 1 as the starting compound and tried to obtain derivatives with improved potency and aqueous solubility for the development of an orally absorbable potent MEK inhibitor.

As the first step of modification of the starting compound, we added the sulfonamide of compound 1 to the hydroxy-piperidine-group. As a result, compounds 2 and 9 in Table 2 showed 17-fold and three-fold increases in MEK1 kinase inhibition compared with compound 1. As the second step, the terminal piperidine-sulfamide was added to various polar substituents to demonstrate the structure–activity relationship of this substructure. The structure–activity relationship was established with two varying positions (R1 and R2 in Table 2). The activities of the piperidine-sulfamide series indicated that a substituent for the chlorine group was desired at the R2 position in cell-based potency rather than for the fluorine or methyl groups, as evidenced by compounds 7–9, 11–13, 16, and SMK-17. The cell-free activities of compounds including fluorine at the R2 position (12 and 16) were more potent than those with a chlorine group (13 and SMK-17). This reversal of potency order between cell-free and cell-based activity is considered to be due to the cell membrane permeability of these compounds. In addition, an alkyl-amine substituent at the fourth (*para*)